SANDIA REPORT
SAND2023-12548
Printed February 2023

Sandia National Laboratories

Technical Justifications for Liquid Hydrogen Exposure Distances

Brian D. Ehrhart, Ethan S. Hecht, Benjamin B. Schroeder

Prepared by
Sandia National Laboratories
Albuquerque, New Mexico
87185 and Livermore,
California 94550

Issued by Sandia National Laboratories, operated for the United States Department of Energy by National Technology & Engineering Solutions of Sandia, LLC.

NOTICE: This report was prepared as an account of work sponsored by an agency of the United States Government. Neither the United States Government, nor any agency thereof, nor any of their employees, nor any of their contractors, subcontractors, or their employees, make any warranty, express or implied, or assume any legal liability or responsibility for the accuracy, completeness, or usefulness of any information, apparatus, product, or process disclosed, or represent that its use would not infringe privately owned rights. Reference herein to any specific commercial product, process, or service by trade name, trademark, manufacturer, or otherwise, does not necessarily constitute or imply its endorsement, recommendation, or favoring by the United States Government, any agency thereof, or any of their contractors or subcontractors. The views and opinions expressed herein do not necessarily state or reflect those of the United States Government, any agency thereof, or any of their contractors.

Printed in the United States of America. This report has been reproduced directly from the best available copy.

Available to DOE and DOE contractors from
U.S. Department of Energy
Office of Scientific and Technical Information
P.O. Box 62
Oak Ridge, TN 37831

Telephone: (865) 576-8401
Facsimile: (865) 576-5728
E-Mail: reports@osti.gov
Online ordering: http://www.osti.gov/scitech

Available to the public from
U.S. Department of Commerce
National Technical Information Service
5301 Shawnee Rd
Alexandria, VA 22312

Telephone: (800) 553-6847
Facsimile: (703) 605-6900
E-Mail: orders@ntis.gov
Online order: https://classic.ntis.gov/help/order-methods/



ABSTRACT

The previous separation distances in the National Fire Protection Association (NFPA) Hydrogen Technologies Code (NFPA 2, 2020 Edition) for bulk liquid hydrogen systems lack a well-documented basis and can be onerous. This report describes the technical justifications for revisions of the bulk liquid hydrogen storage setback distances in NFPA 2, 2023 Edition. Distances are calculated based on a leak area that is 5% of the nominal pipe flow area. Models from the open source HyRAM+ toolkit are used to justify the leak size as well as calculate consequence-based separation distances from that leak size. Validation and verification of the numerical models is provided, as well as justification for the harm criteria used for the determination of the setback distances for each exposure type. This report also reviews mitigations that could result in setback distance reduction. The resulting updates to the liquid hydrogen separation distances are well-documented, retrievable, repeatable, revisable, independently verified, and use experimental results to verify the models.

ACKNOWLEDGEMENTS

This work was done in collaboration with the NFPA 2 Storage Task Group, and the authors wish to thank all the members of the Task Group and NFPA Hydrogen Technologies Technical Committee for their helpful comments, discussion, and feedback.

The authors want to especially thank the following task group members for their critically important input, direction, discussion, and feedback:

David Farese (Air Products),

Derek Miller (Air Products),

Thomas Drube (Chart Industries),

Mukesh Trivedi (Chart Industries),

John Anicello (Chart Industries),

Dusty Brooks (Sandia National Laboratories),

Jamal Mohmand (formerly at Sandia National Laboratories, now at Lockheed Martin), and

Chris LaFleur (Sandia National Laboratories).

This work was supported by the Department of Energy Office of Energy Efficiency and Renewable Energy Hydrogen and Fuel Cell Technologies Office, as part of the Safety Codes and Standards program under the direction of Laura Hill.

CONTENTS

Abstract....3

Acknowledgements....4

Executive Summary....9

Acronyms and Terms....11

1. Introduction....13
   - 1.1. Previous Approach and Justification....13
     - 1.1.1. History of Hydrogen Separation Distances in NFPA Codes....13
     - 1.1.2. Gaseous Hydrogen Separation Distances in NFPA 2....14
     - 1.1.3. Liquid Hydrogen Separation Distances in NFPA 2....14
   - 1.2. Methodology for Bulk Liquid Hydrogen Storage Separation Distances....14
   - 1.3. Document Overview and Organization....15
2. Hole Size Justification....17
   - 2.1. Risk-Informed Equivalent Hole Size....17
     - 2.1.1. Representation of LH2 System....17
     - 2.1.2. Physics Models....18
     - 2.1.3. Risk-Based Distance Calculation....18
     - 2.1.4. Consequence Modeling....20
     - 2.1.5. Equivalent Fractional Hole Size Analysis....20
     - 2.1.6. Sensitivity Study....22
   - 2.2. Bayonet Connector Leak Size....25
   - 2.3. Summary/Conclusions....26
3. Model Comparisons and Justification....27
   - 3.1. Orifice Flow....27
   - 3.2. Unignited Dispersion....29
   - 3.3. Jet Flame Length and Heat Flux....31
   - 3.4. Unconfined Overpressure....32
   - 3.5. Summary of Model Selection and Comparison....32
4. Harm Criteria Selection and Justification....33
   - 4.1. Unignited Concentration....33
   - 4.2. Jet Fire Heat Flux....34
   - 4.3. Peak Overpressure....34
   - 4.4. Summary of Harm Criteria....35
5. Setback Distance Calculations....37
   - 5.1. Calculation Method....37
   - 5.2. Exposure Group Setback Distance Calculations....40
   - 5.3. Resulting Setback Distance Calculation Tables....42
6. Mitigations Justification....45
   - 6.1. Passive Mitigations: Walls....45
   - 6.2. Active Mitigations: Automatic Shutoff Valve....46
     - 6.2.1. Heat Flux Exposure Time....46
     - 6.2.2. Time to Ignition....47
     - 6.2.3. Ignition Probability....48
   - 6.3. Summary and Conclusions....49

7. Summary and Conclusions 51
7.1. Summary 51
7.2. Technical Committee Criteria 52
7.3. Future Work 53
7.3.1. Incorporation of More and Better Data 53
7.3.2. Explicit Consideration of Mitigations and Uncertainty 54
7.3.3. Application of Methodology to Other Systems 55
References 57
Appendix A. Details of Risk-Informed Equivalent Hole Size Calculations 61
A.1. Constant Parameter Values used in QRA 61
A.2. Representative LH2 System 61
A.3. Discontinuities in Equivalent Fractional Hole Size Responses 62
A.4. Consequence-Based Equivalent Hole Size Calculation 63
A.5. Consequence Model Sensitivity 64
A.6. Tabulated Equivalent Fractional Hole Size Results 67
Appendix B. Details of Bayonet Connector Leak Geometry 69
B.1. Methodology 69
B.2. Results and Discussion 70
Distribution 73

LIST OF FIGURES

Figure 1: Example risk contour based on HyRAM+ risk calculations for representative LH2 system 19
Figure 2: Risk-based distances for a range of pipe sizes when using nominal inputs to QRA 21
Figure 3: Equivalent fractional hole size for a range of pipe sizes when using nominal inputs to QRA. Separate line shown for each consequence metric. 21
Figure 4: The limiting equivalent fractional hole size over a range of pipe sizes when using nominal inputs to QRA. Response line shown is the minimum of three consequence models for each pipe diameter. 22
Figure 5: Tornado plot representation of sensitivity of risk based setback distance calculations to parameters included in sensitivity study 24
Figure 6: Equivalent fractional hole size as a function of pipe diameters. Each line represents a separate case in the sensitivity study and is the minimum equivalent fractional hole size of the three consequence metrics considered. 25
Figure 7: Calculations of mass flux for implementations of MLM and HEM models 28
Figure 8: Mass fluxes for different experiments comprared to predictions 29
Figure 9: Experimental data of observed concentration (solid lines) [9] compared to HyRAM+ predictions (dashed lines) at several distances from a horizontal release of LH2 30
Figure 10. HyRAM+ heat flux predictions (shading and solid contour lines) vs data (points) for the DNV-GL test 6 flame [9], with the left-hand plot showing the predicted heat flux at the sensor height (1.2 m), and the right-hand plot showing the bird's eye view predicted heat flux. ..31
Figure 11. Peak overpressures observed after ignition of DNV-GL's test 6 (points) [9] as well as those predicted by HyRAM+ (shading and contour line). 32
Figure 12: Unignited concentration plume from a steady-state saturated liquid hydrogen leak through an 8.5 mm (0.3 in) circular orifice (5% leak area of a 38 mm [1.5 in] pipe) at 414 kPa (60 psi) gauge pressure 38

Figure 13: Jet flame heat flux contours for an ignited, steady-state, saturated liquid hydrogen leak through an 8.5 mm (0.3 in) diameter (5% leak area of a 38 mm [1.5 in] pipe) circular orifice at 1,091 kPa (158 psi) gauge pressure, with 0.9 relative humidity and a horizontal wind speed of 5 m/s. The black line shows the jet flame streamline up to the visible flame length. The top-left plot shows a side-on view, the top-right plot shows an end-on view, and the bottom-left plot shows a top view. 39
Figure 14: Unconfined overpressure resulting from delayed ignition of a steady-state saturated liquid hydrogen leak through an 8.5 mm (0.3 in) circular orifice (5% leak area of a 38 mm [1.5 in] pipe) at 414 kPa (60 psi) gauge pressure. The top-left plot shows a side-on view, the top-right plot shows a side-on view, the top-right plot shows an end-on view, and the bottom-left plot shows a top view. 40
Figure 15: Setback distances for exposure Group 1 41
Figure 16: Setback distances for exposure Group 2 41
Figure 17: Setback distances for exposure Group 3 42
Figure 18: Probability of fatality at different heat flux values for different exposure times 47
Figure 19: Time to ignition for different building materials (using values from [34]) 48
Figure 20: CGA P-28 2014 typical system flow diagram [5] adopted as representative LH2 system for QRA calculations. Blue symbols indicate LH2 components, green symbols indicated GH2 components, and purple symbols indicated components under vacuum. 62
Figure 21: Demonstration of how discontinuities in mass flow rate based ignition probabilities cause jumps in ignition probability over pipe diameter range considered for the QRA analysis. Ignition probabilities only shown for 10.0% leak size. 63
Figure 22: Equivalent hole size as a function of setback distances while varying a range of parametesr impacting concentration metric based risk calculations. 64
Figure 23: Equivalent hole sizes as a function of setback distances while varying a range of parameters impacting heat flux metric based risk calculations 64
Figure 24: Equivalent hole sizes as a function of setack distances while varying a range of parameters impacting heat flux metric based risk calculations 65
Figure 25: Tabulated equivalent fractional hole sizes over a range of inner pipe diameter results. Results correspond to lines shown in Figure 6. Colors are a visual guide to higher (blue) and lower (red) values. 67
Figure 26: Example schematic of a bayonet-style connector used in the transfer of liquid hydrogen 69
Figure 27: Fractional leak area based on O-ring failure of bayonet connector compared to corresponding inner flow diameter 71

LIST OF TABLES

Table 1: Part counts of representative LH2 system 17
Table 2: Risk and consequence metric values used in calculations 20
Table 3: Elements of QRA analyses varied in sensitivity study 23
Table 4: Measured maximum and calculated average concentrations in the far-field for the PRESLHY experiments [8] 30
Table 5: Representative pressure values used for each pressure range in calculation of setback distances 37
Table 6: Minimum distance from outdoor bulk liquefied hydrogen systems to exposures for typical pipe inner Diameter 38.1 mm (1.5 in) 43

Table 7: Minimum distance from outdoor bulk liquefied hydrogen systems to exposure by maximum inner diameter....43
Table 8: Constant parameters in QRA analysis....61
Table 9: Parts counts of representative LH2 system....61
Table 10: Ignition Probabilities [36]....63
Table 11: Bayonet connector diameters and leak area fractions for O-ring failure....70

EXECUTIVE SUMMARY

A table of separation distances for bulk liquid hydrogen storage is provided in the National Fire Protection Association (NFPA) Hydrogen Technologies Code (NFPA 2). These separation distances provide protection to people and buildings if a hydrogen leak should occur. This work describes updated separation distances that are included in the 2023 edition of NFPA 2 as well as the justification for the separation distances.

The logic and calculations are similar to the risk-informed separation distances for bulk gaseous hydrogen that are included in NFPA 2. Risk-informed separation distances utilize insights and justifications from a probabilistic risk assessment but are not solely based on the results of the risk assessment (risk-based). Risk-informed separation distances are not meant to eliminate risk, but rather to limit the risk to an acceptable level; these separation distances alone may not be adequate protection against very unlikely worst-case scenarios, and are meant to work in conjunction with the many other safety-related requirements in a fire code. Similar to the bulk gaseous hydrogen setback distances, a leak size was chosen for bulk liquid hydrogen systems that was informed by various risk assessment methods; this leak size serves as a proxy for those more detailed and variable risk assessments and allows consequence-based distances to be calculated based on selected physical criteria. Similar to the bulk gaseous hydrogen setback distance table, the exposures were grouped into exposure groups, and applicable physical harm criteria were chosen for each exposure group. Finally, and again similar to the bulk gaseous hydrogen setback distance table, setback distances were calculated based on the chosen leak size and harm criteria for variable pipe sizes and system pressures, rather than the quantity of liquid hydrogen stored.

First, a characteristic leak size was determined. A quantitative risk assessment was performed using the Hydrogen Plus Other Alternative Fuels Risk Assessment Models (HyRAM+) software toolkit for a representative liquid hydrogen storage system. The risk assessment calculation considers system pipe size and pressure, leak frequencies for different leak sizes, likelihood of whether the leak is detected and isolated, probability of ignition (either immediate or delayed), and then calculates the likelihood of fatality due to these different outcomes for a position of interest. This risk assessment was performed for multiple pipe sizes and multiple locations to determine the distance from the leak at which a risk criterion (2×10^{-5} fatalities per year, based on the guideline used for gaseous hydrogen setbacks, which was chosen to be consistent with the risk at existing gasoline stations) was met. Consequence-based models in HyRAM+ were then used with the selected exposure group criteria to estimate an equivalent hole size that would lead to the same distance as determined by the full quantitative risk assessment; this led to an equivalent fractional hole size based on the system pipe size. A number of significant inputs to the risk assessment were then varied in a sensitivity study, including system pressure, system temperature, detection and isolation credit, different inputs to the thermal heat flux and overpressure harm models, and different fatality probability models. Almost all of these sensitivity cases resulted in equivalent fractional hole sizes that were <10% of flow area, and most were <5% of flow area. Based on this assessment, a 5% fractional hole size was deemed as a representative, and conservative choice for the leak size. A separate analysis of commercially available bayonet connectors for use in liquid hydrogen transfer operations (a scenario identified as specifically of interest in the 2020 edition of NFPA 2) found that even complete O-ring failure would also be expected to yield leak sizes of approximately 5% or less of flow area.

The physical models in HyRAM+ were then verified and validated to ensure that they result in realistic predictions of cryogenic hydrogen dispersion, flames, and overpressure. The flow rates predicted by the HyRAM+ model tend to be equal to or greater than the values measured in two

experimental data sets. The model for unignited dispersion from liquid hydrogen sources was also compared to two data sets. The streamline distance to an 8% mole fraction was shown to be an accurate or slightly conservative estimate of the experimental observations. There was only a single set of heat flux data from a liquid hydrogen flame that was compared to the HyRAM+ model, but the birds-eye views of the heat fluxes were shown to be conservative relative to the experimental measurements. Wind was not considered for the unignited dispersion models but was considered for the horizontal flame momentum; in both cases, this is a conservative assumption. Finally, the unconfined overpressure model was compared to a single set of liquid hydrogen experiments; the overpressures were significantly overpredicted by the model, resulting in conservative distance predictions to overpressure values. In short, the separation distances calculated by HyRAM+ result in accurate or conservative predictions, albeit with limited liquid hydrogen data for validation.

Physical harm criteria were used with the hole size and physical release models to estimate the distance to a given level of hazard. Unignited concentrations, heat flux from a jet fire, visible flame length, and peak overpressure were all considered for the three exposure groups. Group 1 exposures include lot lines and air intakes and should yield negligible risk to buildings or people. An 8% by volume unignited concentration was selected, based on the ability to sustain ignition, as well as a 4.732 kW/m^2 heat flux and 7 kPa (1 psi) peak overpressure based on negligible risk of fatalities to people. Group 2 exposures include exposed persons not servicing the system and parked cars and should prevent fatalities for people on the site itself although there may be some risk of injury. A heat flux of 9 kW/m^2 was selected for Group 2 exposures, as well as a 13.7 kPa (2 psi) peak overpressure. Finally, Group 3 exposures should prevent fatalities to people, significant damage to buildings, and prevent fire spread that would make an incident worse. A heat flux of 20 kW/m^2 was selected for Group 3 exposures, as was the visible flame length and a peak overpressure of 20.7 kPa (3 psi). Some of these criteria are similar to those used previously in NFPA 2 for gaseous hydrogen, although some have been updated and overpressure is now explicitly considered.

Using the selected leak size, the verified and validated models, and the selected criteria, two tables of setback distances were developed, similar to the format of the gaseous setback distance tables. One table shows the distances for each group of exposures, for three pressure ranges, for a typical pipe size, and the other relates the distances to both system operating pressure and pipe size. While the overall process for developing these distances was similar to and informed by the prior methodology for bulk gaseous hydrogen, there are some differences. One is the elimination of a 1.5 (50%) safety factor, that had been applied to the calculations of the bulk gaseous hydrogen setback distances when the leak size was reduced from 3% to 1%. An implicit safety factor in this analysis arises from the conservative 5% leak size and the conservative distances predicted by the models, much like the initial, conservative 3% leak size for bulk gaseous setback distances.

Mitigations to reduce the setback distances were also considered. Walls can provide a direct barrier between a hazard and a potential person or building. Prior analyses have suggested that walls can reduce risk and thereby can reduce the setback distances. These same reductions would certainly still apply here, given the similarities between the prior gaseous hydrogen setback distance revisions and the current work. There are a number of potential benefits to active mitigations like an automatic shutoff system. However, at this point, it is not clear how to consistently quantify the benefit to hazard reduction for all the relevant hazards considered for setback distance calculation. The requirement to have an automatic shutoff system for bulk liquid hydrogen tanks at public refueling stations is included in the 2023 edition of NFPA 2, which helps reduce the overall risk, even if there is no direct reduction in setback distances.

ACRONYMS AND TERMS

Acronym/Term	Definition
BST	Baker-Strehlow-Tang
CFR	Code of Federal Regulations
CGA	Compressed Gas Association
EFHS	equivalent fractional hole size
GH2	gaseous hydrogen
HEM	homogeneous equilibrium model
HyRAM+	Hydrogen Plus Other Alternative Fuels Risk Assessment Models
LH2	liquid hydrogen
LNG	liquefied natural gas
MLM	metastable liquid model
NFPA	National Fire Protection Association
OSHA	Occupational Safety and Health Administration
PLL	potential loss of life
PRESLHY	Prenormative Research for Safe Use of Liquid Hydrogen
QRA	quantitative risk assessment

This page left blank

1. INTRODUCTION

Hydrogen systems have multiple layers of safety built into the design of the system itself, how the system should be used, and where the system should be located relative to people and buildings. These requirements are defined in a number of different regulations, codes, and standards that pertain to different aspects of system design and operation. Setback distances define a prescribed distance between a potentially hazardous system and different types of other systems, people, buildings, or materials that may be exposed to that hazard. Setback distances can also work in reverse, to protect the hazardous system from external exposures that may damage the system and lead to a release of hazardous material. Risk-informed separation distances are not meant to completely eliminate risk, but rather to limit the risk to an acceptable level; these separation distances alone may not be adequate protection against very unlikely worst-case scenarios. These distances are in addition to many of the other necessary safety design features of the system and are meant to mitigate the risk associated with a potential release. Setback distances have a direct impact on the siting and location of a system within a facility, and often define where something like a hydrogen system could be located. Therefore, it is critical that the setback distances be based on a solid technical justification so that these requirements promote safety; at the same time, the distances should not be unnecessarily onerous that they exclude hydrogen systems from all but the most ideal sites.

Setback distances that apply to many systems in the U.S. are specified in the National Fire Protection Association (NFPA) Hydrogen Technologies Code (NFPA 2) [1]. NFPA 2 contains separation distances for both gaseous and liquid hydrogen, for bulk and non-bulk storage systems, and for gaseous and liquid hydrogen dispensers. Bulk hydrogen storage systems for both gaseous and liquid hydrogen contain the most restrictive (i.e., largest) separation distances, as they pertain to the highest potential consequence release. This work focuses on bulk liquid hydrogen storage setback distances, as they were the most restrictive and lacked a clear basis.

1.1. Previous Approach and Justification

A clear understanding of the requirements for bulk gaseous and bulk liquid hydrogen separation distances is important as a basis for changing these requirements. The work presented herein follows similar reasoning behind bulk gaseous separation distances.

1.1.1. History of Hydrogen Separation Distances in NFPA Codes

The Occupational Safety and Health Administration (OSHA) defines requirements for hydrogen systems in 29 Code of Federal Regulations (CFR) 1910.103. The criteria established in the OSHA tables of distances are based on the 1969 edition of NFPA 50A, the Standard for Gaseous Hydrogen Systems at Consumer Sites [1]. Subsequent editions of NFPA 50A were adopted in 1973, 1978, 1984, 1989, 1994, and 1999, but the OSHA requirements in 29 CFR 1910.103 did not change. In 2003, NFPA 50A was integrated into NFPA 55, the Compressed Gases and Cryogenic Fluids Code, because the committee believed that one standard covering storage and use of all compressed gases and cryogenic fluids was needed [1]. A significant revision to the gaseous hydrogen separation distances was done for the 2010 Edition of NFPA 55, and these revisions were extracted into the first edition (2011) of NFPA 2.

1.1.2. Gaseous Hydrogen Separation Distances in NFPA 2

An evaluation of bulk gaseous hydrogen system separation distances was performed by a Task Group that comprised members of the NFPA 2 Hydrogen Technology Technical Committee in the time period of 2005–2010. This resulted in significant changes to the bulk gaseous hydrogen setback distance tables, using quantitative risk assessments to inform decisions on a new basis for the table [2]. Specifically, the tables were changed to be based on the pressure and pipe size of the system, rather than the total quantity stored. The logic was that while the quantity stored would affect the duration of a leak, the leak size is proportional to the system piping size (i.e., larger pipes, larger leaks) and that the pressure behind the leak affects the distance over which a hazard extends (e.g., higher pressures result in larger flames). Additionally, exposures were grouped so that similar exposure types could be considered with the same criteria, rather than establishing different setback distances for each individual exposure. These changes were applied to the first edition of NFPA 2 in 2011. Criteria used in the setback distance table calculations, table format, and exposures have continued to evolve and were revised for the 2020 editions of NFPA 2.

1.1.3. Liquid Hydrogen Separation Distances in NFPA 2

The table of separation distances for bulk liquid hydrogen storage have remained largely unchanged for many recent editions of both NFPA 55 and NFPA 2. These setback distance tables determine the setback distances based on the volume of liquid hydrogen stored in the system, similar to how the gaseous hydrogen setback distance tables were defined before the first edition of NFPA 2.

For the 2020 editions of NFPA 2 and NFPA 55, a task group considered revisions for the bulk liquid hydrogen storage setback distance tables. It was ultimately decided that the work was not ready for that edition of the code, but did result in NFPA 2 Annex I.8, which identified a proposed path forward. This proposed methodology highlighted the use of a representative liquid hydrogen storage system (such as that given in the Compressed Gas Association (CGA) P-28, Risk Management Plan Guidance Document for Bulk Liquid Hydrogen Systems) and the use of risk assessments on that system to inform revisions to the setback distance table. The task group specifically highlighted transfers of liquid hydrogen from a transfer truck to a bulk liquid hydrogen tank as of particular concern.

1.2. Methodology for Bulk Liquid Hydrogen Storage Separation Distances

A task group of the NFPA 2 Hydrogen Technology Technical Committee reviewed the previous liquid hydrogen setback distances and considered how a similar methodology to that used for bulk gaseous hydrogen setback distances could be applied to bulk liquid hydrogen setback distances, which is described here. Similar to the bulk gaseous hydrogen setback distances, a leak size was chosen that was informed by risk assessments; this leak size serves as a proxy for those more detailed and variable risk assessments and allows consequence-based distances to be calculated based on selected physical criteria. Much like the bulk gaseous hydrogen setback distance table, the exposures were grouped into exposure groups, and applicable physical harm criteria were chosen for each exposure group. Finally (and again like the bulk gaseous hydrogen setback distance table) setback distances were calculated for bulk liquid hydrogen storage systems based on the chosen leak size and the chosen harm criteria for a range of typical pipe sizes and system pressures, rather than the quantity of liquid hydrogen stored.

1.3. Document Overview and Organization

This document describes the technical justifications for the revisions of the bulk liquid hydrogen storage setback distances in the 2023 edition of NFPA 2. First, this Introduction (Section 1) summarizes previous approaches and broadly describes the current approach for these revisions. Section 2 provides a justification for the hole size that forms the basis of the leak calculations to obtain the setback distances. Section 3 describes the numerical models used for calculation of the setback distances and compares the model results to similar models and experimental data. Section 4 justifies the harm criteria used for the determination of the setback distances for each exposure type. Section 5 describes the setback distance calculations and presents the values. Section 6 reviews possible mitigations that could result in smaller setback distances. Finally, Section 7 summarizes the entire methodology and results, identifies potential improvements to the process, and describes how this process could be applied for other separation or hazard distances.

This page left blank

2. HOLE SIZE JUSTIFICATION

The setback distances in this analysis are based on numerical physical models of the consequences of a leak of liquid hydrogen. Therefore, a leak size must be determined in order to provide the basis for the leak simulation that will determine the resulting setback distance. There are many potential ways in which such a leak size could be determined; this analysis considers a novel risk-informed equivalent hole size as a basis. Additionally, this hole size is also compared to the physical geometry of an O-ring failure leak to calibrate whether this hole size is reasonable.

2.1. Risk-Informed Equivalent Hole Size

A quantitative risk assessment study was used to inform the determination of setback distances. Risk-informed separation distances utilize insights and justifications from a risk assessment, but are not solely based on the results of the risk assessment (i.e., not risk-based). In this analysis, an example LH2 storage system was analyzed. A quantitative risk assessment (QRA) was performed on this system to determine the distance a person would need to be from the system at which a selected individual risk criterion was met. This risk assessment considered multiple different leak sizes, the likelihood of each leak size, and the probability of fatality from each leak size. Once this risk-based distance was obtained, an equivalent leak size was the calculated based on direct hazard (consequence-based) models that would give the same distance to the hazard distance as to the risk-based distance. A sensitivity study was then performed to vary many different inputs and assumptions in the risk assessment in order to see how the resulting equivalent leak sizes would vary. Finally, a specific leak size was selected which was informed by this ensemble of equivalent leak sizes.

HyRAM+ version 4.1 [3] was used to perform all of the modeling. Both risk and physical consequence modeling capabilities are contained within HyRAM+ and both are utilized to perform QRAs. The remainder of this subsection provides an overview of the analysis performed to inform the setback distances; additional analysis implementation details can be found within Appendix A. Details about the specific models utilized within HyRAM+ can be found within the technical reference manual [4].

2.1.1. Representation of LH2 System

While liquid hydrogen storage systems will vary in terms of components used and process flows based on application, the CGA P-28 (2014 edition) [5] system configuration was selected as a representative baseline system. From the CGA P-28 system, components with which liquid hydrogen interacts were included in the analysis; components that interact with gaseous hydrogen or vacuum were not included. The baseline LH2 system included the components listed in Table 1; the vaporizer was not included because the analysis was focused on the bulk liquid hydrogen system alone.

Table 1: Part counts of representative LH2 system

Component	Count
Compressors	1
Filters	2
Flanges	8

Component	Count
Instruments	3
Pipes	10
Valves	44
Vessels	1

Within the representative system, a single pipe size was assumed with a 1.7 inch outer diameter and a 0.1 inch wall thickness, resulting in a 1.5 inch inner diameter. The fuel within the system is 100% liquid hydrogen at a pressure of 827 kPa (120 psi) absolute pressure and assumed to be saturated liquid upon release through a leak. Leaks are assumed to be horizontal through circular holes with a discharge coefficient of 1. These conditions are used at the leak point itself; no additional piping effects are considered. This is expected to be a conservative assumption, as accounting for piping effects would reduce the density of the hydrogen, leading to a lower release rate. The environment surrounding the system was assumed to be 20°C with 90% relative humidity and at sea level pressure (101.325 kPa).

2.1.2. Physics Models

Reduced order physics models from the HyRAM+ toolkit are used to model leaks and associated consequences for the hydrogen system [4]. To represent leaks from LH2 systems, the choked flow through the leak orifice is first modeled based on the state of the fuel and characteristics of the orifice. Next, the evolution of the flow as it transitions from a momentum-based jet to a diffuse buoyant plume is captured and used to estimate steady-state concentration profiles. Although emptying of an LH2 system through a leak is a transient process in which the pressure and flow rate decays over time, a steady state flow from the maximum pressure was assumed. To determine the potential heat flux from a jet fire, it is assumed that the leak is ignited and the resulting steady state flame is modeled along with the resulting heat fluxes to surrounding locations. A diffusion flame model is used to represent the steady state flame. The non-ignited steady-state leak flow response is used to determine the location and quantity of fuel available in the case of delayed ignition. The overpressure and impulse resulting from this delayed ignition are also input to the risk calculation.

2.1.3. Risk-Based Distance Calculation

To model risk for LH2 storage systems, the likelihood of a leak occurring is multiplied by the consequence of the leak. This calculation is repeated for a range of possible leak sizes, resulting in risk values for each leak size and outcome. Risk for the system is the sum of all the leak size and outcome risks. Here the consequence of a leak is measured in terms of annual fatalities and risk is calculated using a potential loss of life (PLL) metric. For each release the probability of different physical outcomes such as leak detection, no ignition, a jet fire, or a delayed ignition are calculated using an event sequence diagram approach. A detection credit is used to specify the probability that a leak is detected and mitigated prior to any adverse consequences. Within the event sequence diagram, the probability of ignition is specified based on the release mass flow rate. For a given system, five leak sizes are considered: 0.01%, 0.1%, 1%, 10%, and 100% of pipe flow area. These fractional leak sizes are applied to the interconnecting piping for all components. Leak frequencies

for each leak size and system component are used to estimate the likelihood of a leak. These leak frequencies were developed based on generic leak frequencies updated with gaseous hydrogen and liquefied natural gas leak frequency data, but no liquid hydrogen-specific data [6]; as such, these parameters are highly uncertain and are varied in the sensitivity study described below. Fault tree logic that accounts for component counts is used to determine the total leak frequency for the entire system for each leak size. An event tree is used to estimate the probability of different outcomes for each leak size, including the possibility of the leak being safely detected and isolated, immediate or delayed ignition occurring, or no ignition occurring. These ignition probabilities were uncertain estimates developed for gaseous hydrogen, and so the ignition probability for liquid or cryogenic hydrogen may be different; for more details, see Appendix A. For each leak size, the resulting jet fire and overpressure events are modeled, providing a spatial understanding of the associated heat flux and peak overpressure responses. The physical effects are estimated for a single individual at different horizontal distances away from the leak point (directly inline with the leak) to estimate the spatial distribution of effects. Fatality probit models for heat flux and overpressure events are then used to determine the spatial distribution of fatality probabilities. Ultimately, fatality probability acts as the leak consequence and when multiplied by the respective leak likelihood and summed over all leak sizes results in a spatially distributed risk.

The risk acceptability metric used for this analysis was 2×10^{-5} fatalities per year, although this value is varied in the sensitivity study (see Section 2.1.6). This risk acceptability metric is based off the value used in the NFPA 2 gaseous hydrogen storage setback distance analysis [2]. This metric was originally selected as a risk guideline for a handful of reasons: it was thought to be consistent with risk at existing gasoline stations, was in general agreement with risk criteria being utilized in several countries, was approximately twice the risk value recommended by the European Industrial Gas Association for hydrogen facilities, represented a low fraction (approximately 5%) of the risk experienced by the public due to all causes, and was roughly equal to the risk imposed by other types of fires [2]. Figure 1 shows the system risk of the representative LH2 system as a function of distance. The point at which the risk response line intersects with the selected risk criterion line determines the distance away from the system at which that accepted risk level is reached. Given this risk metric, the distance away from the system at which this risk value is realized for the representative LH2 system is 13.6 m for the base-case scenario.

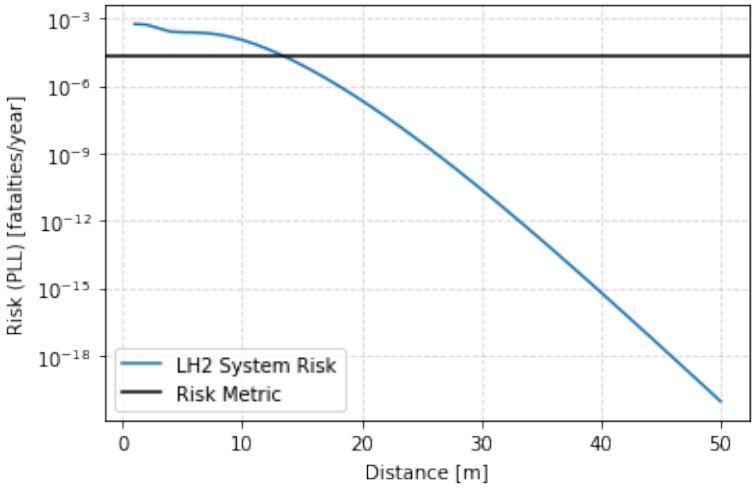


Figure 1: Example risk contour based on HyRAM+ risk calculations for representative LH2 system

2.1.4. Consequence Modeling

Consequence models were used to estimate setback distances based on physical criteria, rather than risk criteria. Three consequence models were utilized based on different physical metrics: hydrogen concentration, heat flux, and peak overpressure. Values for those three metrics were for exposure Group 1 (see Section 4) and are provided in Table 2. The calculation of the setback distance for the consequence models is described in Section 5.

Table 2: Risk and consequence metric values used in calculations

Metric	Value
Risk	2×10^{-5} fatalities/year
Concentration	8% by volume
Heat Flux	4.732 kW/m^2
Peak Overpressure	6.895 kPa (1 psi)

2.1.5. Equivalent Fractional Hole Size Analysis

A risk-based distance alone can be very sensitive to system specifics (see Section 2.1.6), which makes it difficult to determine a risk-based prescriptive requirement. Instead, an equivalent fractional hole size (EFHS) approach was developed. First, risk-based distances (as described in Section 2.1.3) were calculated for a range of pipe sizes, as shown in Figure 2. The range of pipe size is expected to span the variety of liquid hydrogen pipe sizes currently in use and was based on input from industry experts in the NFPA Hydrogen Storage Task Group. The step-change discontinuity in Figure 2 and subsequent figures is due to the ignition probability value changing with mass flow rate of the leak, as discussed in Appendix A.3.

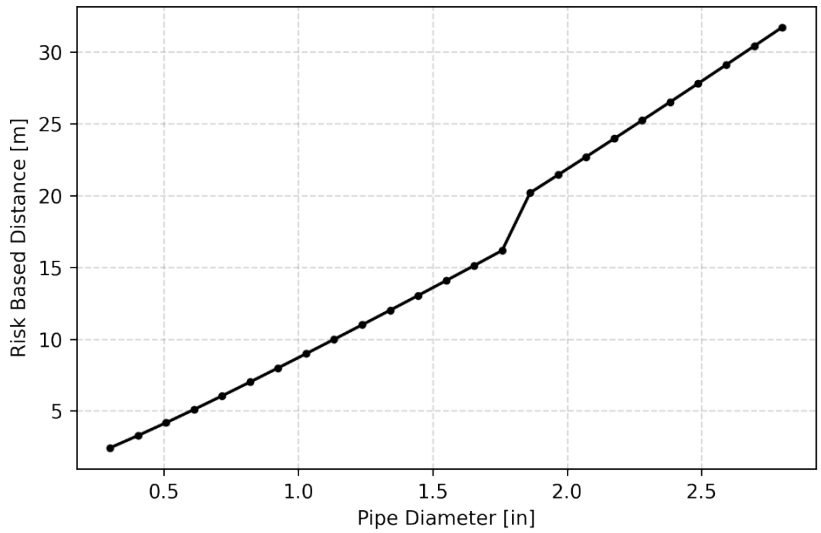


Figure 2: Risk-based distances for a range of pipe sizes when using nominal inputs to QRA

Once risk-based distances were obtained, the three consequence models were then used to calculate the equivalent hole size that would result in the respective consequence metric (see Table 2) being met at the same distance as each risk-based distance. In order to generalize results, the flow area for the equivalent hole size was divided by the flow area of the specified system pipe size to determine the EFHS. This results in an EFHS for each consequence metric over a range of pipe sizes, as shown in Figure 3.

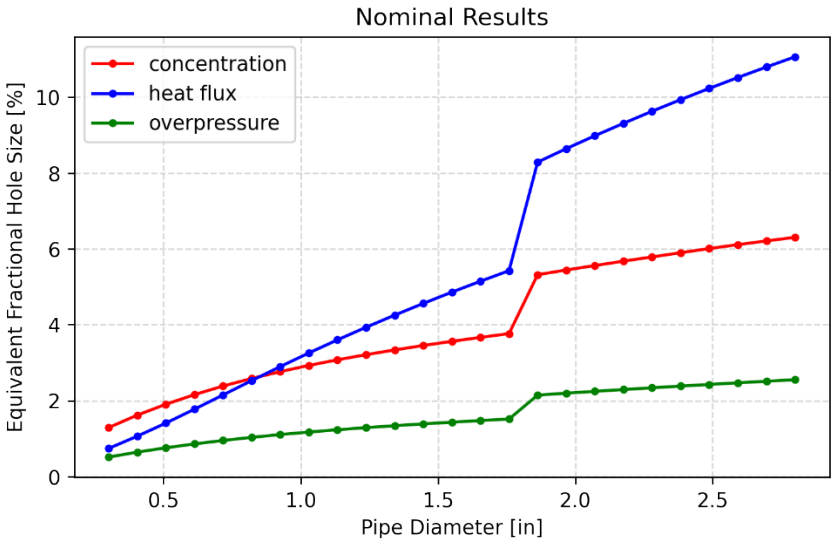


Figure 3: Equivalent fractional hole size for a range of pipe sizes when using nominal inputs to QRA. Separate line shown for each consequence metric.

For each pipe size the smallest EFHS among the three consequence models is the limiting value. Determining this minimum for a range of pipe sizes results in a single functional relationship between EFHS and pipe size. Figure 4 shows the resulting minimum curve derived from the three

consequence curves in Figure 3. For this particular example, the overpressure curve has the minimum EFHS values, and so the overpressure curve results in the curve shown in Figure 4. However, in other scenarios, other hazards may be dominant, and so the resulting minimum curve may be based on other hazard curves. The minimum EFHS curve for the set of consequence criteria is used because it relates the limiting consequence-based criteria to the risk-based distances obtained. This is analogous to how the final setback distance calculations use the largest distance of the hazard criteria calculated (see Section 4).

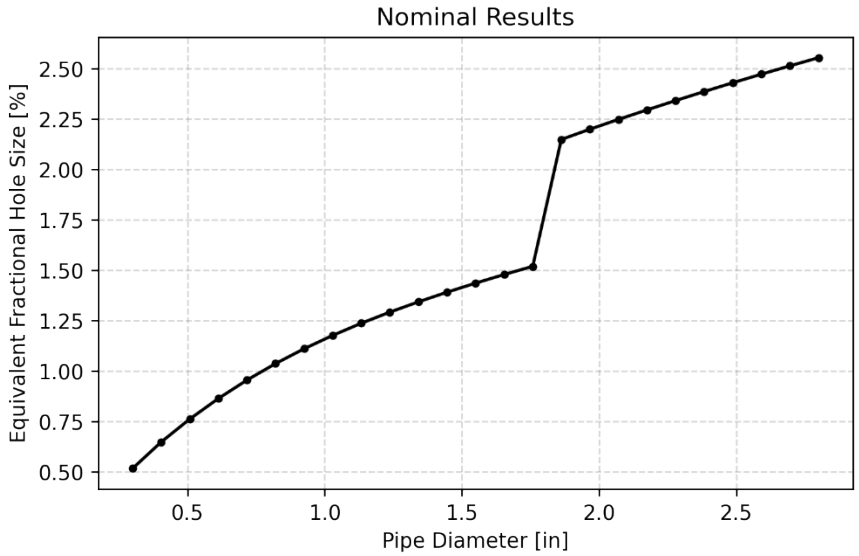


Figure 4: The limiting equivalent fractional hole size over a range of pipe sizes when using nominal inputs to QRA. Response line shown is the minimum of three consequence models for each pipe diameter.

2.1.6. Sensitivity Study

In order to account for uncertainty in the QRA calculations due to analysis assumptions, a sensitivity study was utilized which examines multiple sensitivity cases. Table 3 shows all the QRA modeling assumptions considered, nominal (base case) values, and bounds explored within the sensitivity study. Each QRA assumption was assigned two bounding values that either numerically bounded the nominal value or represented alterative options for the assumption. For instance, the detection credit bounds were 0.0 and 0.95, which respectively represent no probability of a leak being detected and 95% probability of it being detected; these values bound the nominal value of 50% detection probability. An example of an alternative option is the peak overpressure probit model selected, where TNO Head, Eisenburg, and HSE are three potential options available within HyRAM+; the TNO Head probit is selected as the most realistic, and is therefore used as the nominal value for most calculations, but the effects of the other models are calculated in the sensitivity cases. For each of the sensitivity cases below, only one input value was changed at a time while all other values were kept at the nominal values.

Table 3: Elements of QRA analyses varied in sensitivity study

	Units	Nominal	Bound 1	Bound 2
Detection Credit	probability	0.50	0.00	0.95
Fuel Phase		Sat. Liquid	Sub-Cooled Liq. (22.3°C)	Sat. Vap.
Exposure Time	s	30.0	15.0	60.0
BST Mach Flame Speed		0.35	0.20	5.2
Fuel Pressure	psia	120	60	187
Ignition Probabilities		1x	0.5x	2x
Risk Metric	fatalities/year	2×10^{-5}	1×10^{-5}	4×10^{-5}
Component Count*	# of components	(69)	Half (34)	Double (138)
Thermal Probit		Eisenberg	Tsao & Perry	TNO
Overpressure Method		BST	TNT	Bauwens/Dorofeev
Relative Humidity	%	90	1	100
Overpressure Probit		TNO Head	Eisenberg	HSE
Discharge Coefficient		1.0	1.0	0.5

** roughly 0.5x and 2x Table 1 values*

To illustrate the sensitivity of QRA calculations to the parameters included in the sensitivity study, risk metric based distances, as shown in Figure 2, were calculated for each sensitivity case and plotted as a tornado plot in Figure 5. Pipe inner diameter is shown as a parameter in the plot to demonstrate the impact of the pipe's size, which varies between 0.3 and 2.8 inches (7.62 to 71.1 mm). The tornado plot results show QRA calculations are highly sensitive to pipe inner diameter due to this effectively driving the mass flow rate of the leak. Both the higher BST Mach Flame speed and Bauwens/Dorofeev overpressure model assume detonation, resulting in large increases to the risk metric based distance. Changing the exposure time directly changes the thermal dose calculated for heat fluxes from a jet fire. Overall, the tornado plot demonstrates the impact of assumptions made in the QRA calculations is informative as to the relative magnitude of importance of the

assumptions, and demonstrates the correlation between changes in each assumption and the risk based distance estimate.

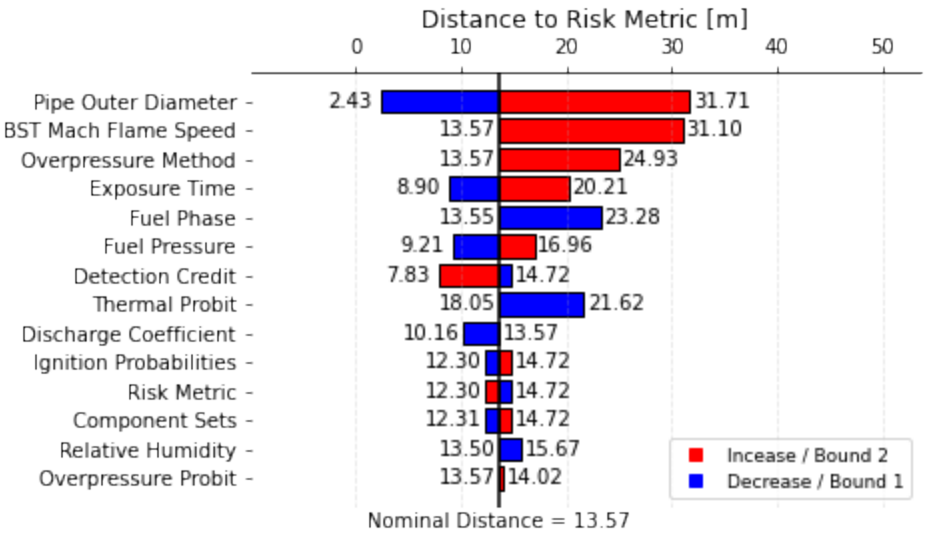


Figure 5: Tornado plot representation of sensitivity of risk based setback distance calculations to parameters included in sensitivity study

A sensitivity study was next utilized with the QRA calculations to generate a population of EFHS curves. For each sensitivity case one QRA calculation assumption (input) was varied resulting in an EFHS curve. Figure 6 shows the population of EFHS curves generated by the sensitivity study. Of the 26 cases included in the sensitivity study, 21 were below a 5% EFHS for the largest inner pipe diameter studied, which supports the selection of this EFHS for use in the setback distance tables. All 5 cases above 5% EFHS were already highlighted as being high sensitivity parameters for the QRA calculations in the risk-based distance tornado plot. The two cases that exceeded 10% EFHS both assumed overpressure models with detonation, which is believed to be unrealistic for the unconfined outdoor release: BST with a 5.2 Mach flame speed and the Bauwens/Dorofeev model. For example, Jallais et al. did not observe detonations in their unconfined overpressure outdoor release experiments [7]. The remaining three cases that exceeded 5% EFHS were all considered to use overly conservative assumptions as well: the leak coming from a sub-cooled liquid source; doubling the exposure time, which doubles the heat flux thermal dose; and using the Tsao and Perry thermal probit model that included infrared effects.

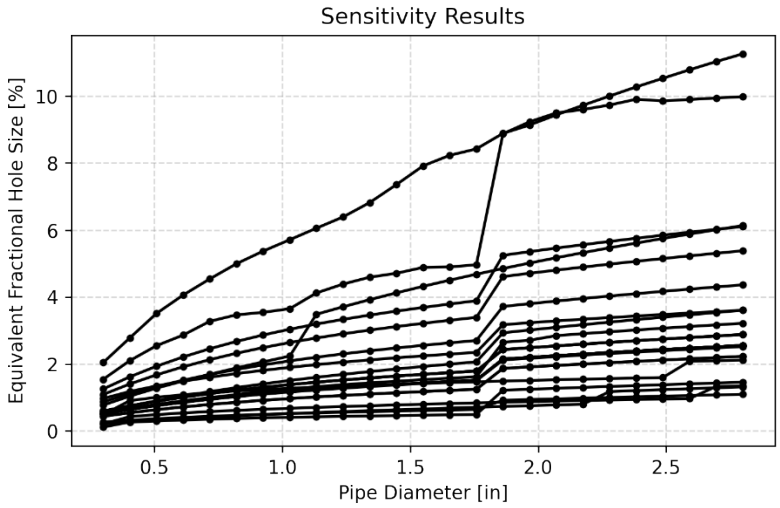


Figure 6: Equivalent fractional hole size as a function of pipe diameters. Each line represents a separate case in the sensitivity study and is the minimum equivalent fractional hole size of the three consequence metrics considered.

A leak of a sub-cooled liquid would greatly increase the density of the leak flow, potentially leading to more severe consequences. However, this modeling defines the source conditions of the fluid (i.e., the liquid hydrogen) at the leak point, not necessarily in the bulk storage. Recent experiments with liquid hydrogen showed difficulty in getting hydrogen in a liquid state to exit an orifice, even though this was the intention of the experimental efforts and the liquid in the storage tank was subcooled [8, 9]. Therefore, because of the warming that can occur between the bulk source of hydrogen and a potential leak point, it is assumed that the leak through an orifice of a sub-cooled liquid is unrealistic.

The exposure time input directly affects the thermal dose and therefore the thermal harm probit calculations in the risk assessment. The default value in HyRAM+ was previously 60 seconds [4], but after reviewing the literature basis for this value, 30 seconds was selected as the nominal value for this analysis. Exposure time should reflect the amount of time it takes an individual to move a sufficient distance away from the flame such that they are no longer being harmed, which will be person dependent. Multiple sources suggested that a 30 second exposure time is an appropriate estimate for this thermal dose and harm calculation [10, 11].

Finally, the Tsao & Perry thermal harm probit includes effects from infrared radiation from nuclear explosions [2, 4]. By contrast, the Eisenberg thermal probit (used as the nominal selection) only considers ultraviolet radiation from explosions. Including infrared effects may be unrealistic for hydrogen fires, which do not radiate as much due to the relative lack of carbon in the flame [12]. Conversely, the other thermal probit sensitivity case used the TNO probit, which is based on the Tsao & Perry model but modified to account for clothing [4]. Therefore, the use of the Tsao & Perry probit, which overpredicts the effects of radiation from hydrogen fires while also not accounting for clothing, is assumed to be unrealistic for this analysis.

2.2. Bayonet Connector Leak Size

One scenario of concern for the NFPA 2 Hydrogen Storage Task Group in the last code revision cycle was a release of hydrogen from the transfer hose, such as when liquid hydrogen is being

delivered from a truck [1]. The point of transfer often has some of the largest pipe/hose diameter, pressure, and flow rate of any point in the system, leading to potentially worse consequences. Additionally, the transfer point has connections that are regularly broken and made for each transfer, meaning that an error in making the connection could lead to a release. Therefore, a failure of the transfer point connection is specifically of interest in determining a relevant leak size for the setback distances. The risk assessment methodology described previously includes all types of leaks, including those from human errors like transfer connections. However, these parameters lack significant data and so are highly uncertain; improving the consideration of transfers would be a useful area of future work.

A review of commercially available bayonet-style connectors for liquid hydrogen transfer was done, and the potential fractional hole size was estimated for each (details of this analysis are given in 0). Specifically, the flow area that would result from an O-ring failure was compared to the cross-sectional flow-area of the connector, which is the same fractional hole size discussed above. Almost all of the fractional leak sizes estimated through the bayonet O-ring failure geometry are below 5%. The single value that is >5% is for a 0.5 inch diameter flow connector, which is smaller than most commonly used piping for liquid hydrogen. Most (18/22) of the fractional leak sizes are below 3%, especially for larger pipe sizes, which suggests that a fractional leak size of 5% should generally be conservative.

2.3. Summary/Conclusions

A risk analysis developed for a representative LH2 storage system was used to determine the distance at which a specified risk metric was met. Equivalent leak hole sizes were then calculated for concentration, heat-flux, and maximum overpressure consequence models based on meeting specified consequence criteria at the same distance as the risk-based distance. EFHS curves were developed by calculating those risk-based distances and resulting equivalent leak sizes for a range of inner pipe sizes and then normalizing by the pipe size. Sensitivity studies were then used to demonstrate the impact of assumptions used in the risk assessment and resulted in an ensemble of EFHS size curves. This sensitivity study resulted in the selection of 5% EFHS as being a conservative, but not unrealistic, basis for LH2 storage system setback distances. The sensitivity study also illustrated the significant impact assumptions can have on quantitative risk analyses. This leak size was compared to potential leak sizes from commercially available LH2 bayonet connectors, and the 5% fractional leak size was again shown to be conservative, but not unrealistic.

3. MODEL COMPARISONS AND JUSTIFICATION

As discussed in Sections 0 and 2, quantitative risk assessment and the calculation of consequence-based separation distances rely on several underlying physical models for hydrogen behavior. It is therefore critical that the models are representative of reality. The models within HyRAM+ version 4.1 were used in this analysis. In this section, each model is compared to experimental data, where possible to justify its use and prove its validity in these calculations.

3.1. Orifice Flow

The first step in any release is the flow through an orifice. In order to calculate this flow, the state of the fluid upstream of the leak must be defined, by two thermodynamic properties, typically pressure and phase (i.e., subcooled liquid at a specified temperature, saturated liquid, two-phase with a specific liquid/vapor fraction, or saturated vapor). For a cryogenic fluid, there are then several modeling assumptions that could be made to calculate the flow through an orifice. Two that were considered were a metastable liquid model (MLM) and a homogeneous equilibrium model (HEM). The MLM assumes that a liquid upstream of a leak will remain a liquid as it flows through the leak Because of the high density liquid flowing through the orifice, the flowrates predicted using this model are high. The HEM on the other hand (in this implementation) assumes that the fluid flowing through the orifice remains isentropic. In most cases, this means that a saturated liquid (or even slightly subcooled liquid) will flash to a two-phase mixture at the throat.

The gas and fluid phases are assumed to flow at the same velocity (homogenously) through the throat. Previous versions of HyRAM+ used a homogeneous equilibrium model to calculate flow through an orifice but relied on a calculation of the speed of sound of the two-phase mixture that formed in the throat as a saturated liquid flashed to two-phase. This calculation is uncertain, as there are challenges in measuring the speed of sound of two-phase flows, especially for cryogenic fluids. Rather than calculating the two-phase speed of sound, HyRAM+ version 4.1 solves for the maximum mass flux through an orifice as the fluid pressure drops isentropically while flowing through an orifice [4]. This calculation method results in the speed of sound for single-phase fluids (and therefore this method is also suitable for gas flows), and relies only on the enthalpy and entropy of the two-phase mixture, a much more reliable calculation than the speed of sound.

This model was first verified against an implementation by Air Products and compared against previous calculations as well as the MLM. This comparison can be seen in Figure 7. As shown, the previous calculation that relied on the speed of sound of a two-phase mixture (dashed blue line) underpredicted the mass flux relative to the current implementation of the HEM. Both the Air Products implementation and the HyRAM+ implementation result in the same mass flux. The MLM predicts much higher mass fluxes than the HEM. The mass fluxes predicted using the MLM could also be reproduced by Chart Industries and Air Products. The MLM and HEM models were compared to experimental data (detailed below) and the MLM model significantly overpredicted the measured flowrates. Because the orifice flowrates were more accurately predicted (or more modestly overpredicted) by the HEM model and this is the same calculation as is used for compressed gaseous flows, the HEM model (with the new maximum mass flux search algorithm) was selected as the flow model in HyRAM+.

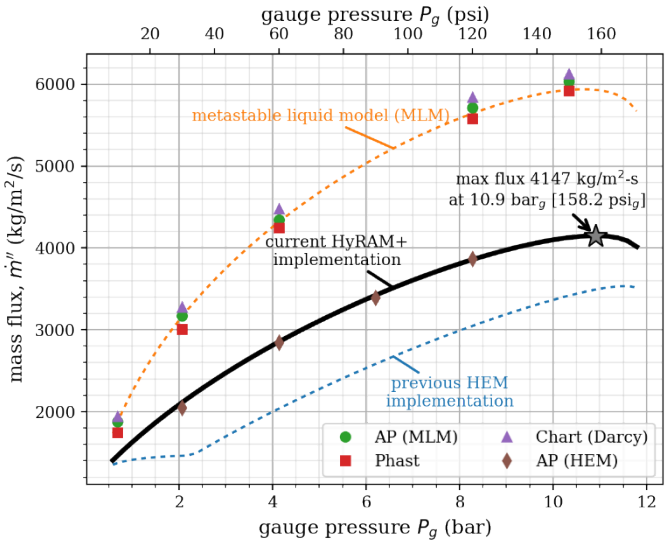


Figure 7: Calculations of mass flux for implementations of MLM and HEM models

Two experimental campaigns, by DNV-GL [9], and by the Health and Safety Executive under the Prenormative Research for Safe Use of Liquid Hydrogen (PRESLHY) project [8], measured the mass flows of liquid hydrogen while performing experiments. These experiments featured several measures of pressure in the tank upstream of the release and just before the release point. The test data is shown as the black bars. The flows predicted in HyRAM+ 4.1, using the tank pressure (as is used in calculation of the separation distances), are shown as the blue striped bars in Figure 8. With the exception of the 5 bar (500 kPa), 6 mm PRESLHY experiment, the mass flux is overpredicted by the model. In this case, the authors [8] show some unsteadiness in the mass flow rate measurements, which they presume was caused by gas bubbles disturbing the measurement, with 10-20% error, as indicated by the red line (15% error is shown here) at the top of the data bar. Using the tank pressure and the HEM is generally conservative as compared to test data. Using HEM model and storage tank pressure to model a leak rate is additionally conservative since a real system will have piping.

The dispersion and flame models are only for gases. After flowing through the orifice, the fluid is assumed to continue with the same mass, momentum, and energy until it reaches atmospheric pressure, begins to entrain air, and flashes to a gas, neglecting any effects from air or humidity condensation [4].

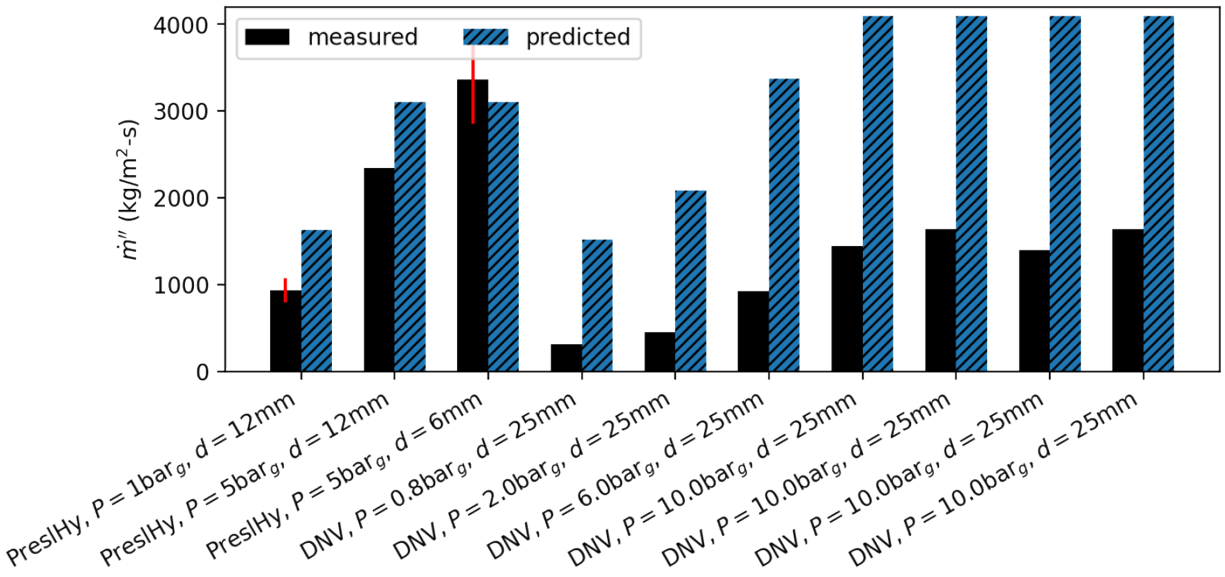


Figure 8: Mass fluxes for different experiments comprared to predictions

3.2. Unignited Dispersion

There were two horizontal releases during the DNV-GL experimental campaign [9], which were repeats of the same experiment. These were both 10 bar tank pressure releases through a 25.4 mm nozzle. Measurements of concentration using oxygen sensors were made at several heights from 0.1–1.8 m above the ground at 30, 50, and 100 m from the nozzle. The maximum concentration at any height at these three radii are shown in Figure 9. There were significant variations in the maximum concentration at different times, owing to the unsteadiness of the wind (6.7 m/s average, 12.1 m/s max for test 4 and 2.7 m/s average, 5.8 m/s max for test 6). For these releases, the concentration dropped below the lower flammability limit somewhere between 50 and 100 m. Test 6 was ignited at about 140 sec, the time at which the mole fractions drop to zero or erroneously read below zero. The HyRAM+ predicted concentrations along the streamline (not at a specific height, and neglecting the effects of wind), shown by the horizontal dashed lines, are lower than the maximum concentration measurements at 30 m for some times throughout the test, but in the far field at 50 and 100 m predicted concentrations are above or equal to those observed.

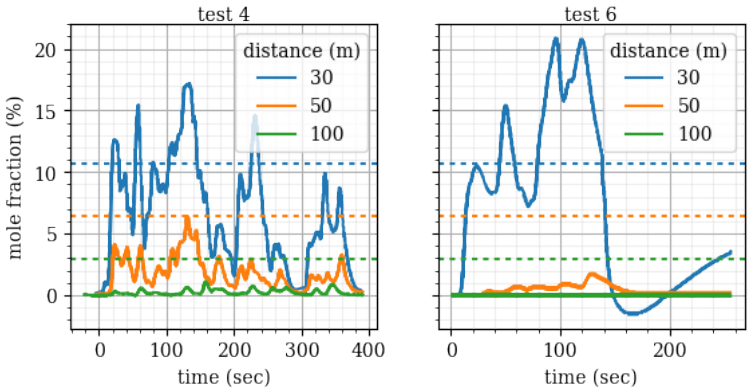


Figure 9: Experimental data of observed concentration (solid lines) [9] compared to HyRAM+ predictions (dashed lines) at several distances from a horizontal release of LH2

The PRESLHY campaign [8] had several measures of unignited concentrations, in both the near-field and the far-field. The far-field data is more relevant to the distance calculations because distances to low concentration values rather than high values are of interest. In the far-field, a sensor was placed 14 m from the releases at a height of 1.5 m. The sensor could measure concentrations up to the lower flammability limit (4%). For the distance calculations to the different harm criteria, the streamline distance to a given concentration is used. Therefore, when comparing to the test data, the concentration predicted by HyRAM+ exactly at the point (14 m, 1.5 m), as well as 14 m along the streamline is presented. In this way, the measured concentrations, which had wind influencing their measurements can be compared to the conservative estimates of distance used to calculate setback distances in this work. The concentrations are compared to the data in Table 4. Buoyancy is evident in the HyRAM+ predictions because the concentrations along the streamline at 14 m are all greater than the concentrations at the point (14 m, 1.5 m). The streamline values overpredict the measured concentrations in all cases, while for the low pressure releases the concentrations at the point (14 m, 1.5 m) tend to be underpredicted. The accuracy of the predictions is likely affected by the wind in the experiments, which ranged from 1.8–3.5 m/s, generally in-line with the releases, which would blow a brief pocket of high concentration fluid past the sensors and increase the observed maximum concentrations. In general, wind will reduce the average concentration of a plume [13].

Table 4: Measured maximum and calculated average concentrations in the far-field for the PRESLHY experiments [8]

Nozzle diameter [mm]	Tank pressure [bar_g]	Measured concentration [vol-%]	HyRAM+ calculated concentration at (14m, 1.5m) [vol-%]	HyRAM+ calculated concentration 14m streamline [vol-%]
25.4	1	>4	18.7	19.6
12	1	>4	3.4	10.0
6	1	2.15	0.01	4.9
25.4	5	>4	18.1	19.2
12	5	>4	9.9	10.0
6	5	3.32	4.8	5.2

3.3. Jet Flame Length and Heat Flux

As described by Hecht and Ehrhart [4], the flame length in HyRAM+ is calculated based on a correlation described by Houf and Schefer [14], with the trajectory calculated using the model described by Ekoto et al. [15]. We were unable to find any data on flame length for liquid hydrogen flames, but the model agreed well with gaseous cryogenic lab-scale flames, as documented by Ehrhart et al. [16]. The flame length and trajectory are subsequently used in the heat flux calculation, so validation of the heat flux prediction is an indication of the flame model accuracy.

There was a single ignited horizontal release during the DNV-GL experimental campaign, test 6 [9]. This was a 10 bar tank pressure release through a 25 mm orifice at a height of 0.49 m. The wind was around 3 m/s nominally in the direction of the release/flame. Radiometers at several locations measured the heat flux from the flame. Figure 10 shows the measured heat fluxes as points and predicted heat flux for an ignited release (jet flame) of 10 bar, saturated liquid hydrogen through a 25 mm orifice at a height of 0.49 m with a 3 m/s wind blowing in the same direction as the flow. The frame on the left shows the heat fluxes at the height of the measurements, 1.2m, while the right-hand frame shows the 'birds-eye' heat flux that is used for setback distance calculations in this work. The 10 points are at the locations of the radiometers and are colored and labeled by the average value of the measurements. The measurements show the highest heat flux at a location of (10 m, 10 m); the wind is likely blowing the flame in the positive y-direction. This angle of the flame is not captured in the modeling. The wind in the modeling (accessed by using the Python back-end of HyRAM+ [4]) does not capture this angle, as the wind is assumed to be directly inline with the release direction. The wind only affects the x-momentum of the flame, causing it to appear to have less buoyancy and remain closer to the ground. HyRAM+ tends to underpredict the highest measured heat fluxes (especially the left-hand figure at the sensor location height), and overpredict the smallest heat fluxes. Focusing on the right-hand frame, the distance from the origin to the x-value of the birds-eye heat flux contours of interest for setback distances (20, 9, and 4.7 kW/m^2) are each further than the distance from the origin to the measured heat fluxes (i.e., a higher heat flux measurement is never found outside the respective dashed circle).

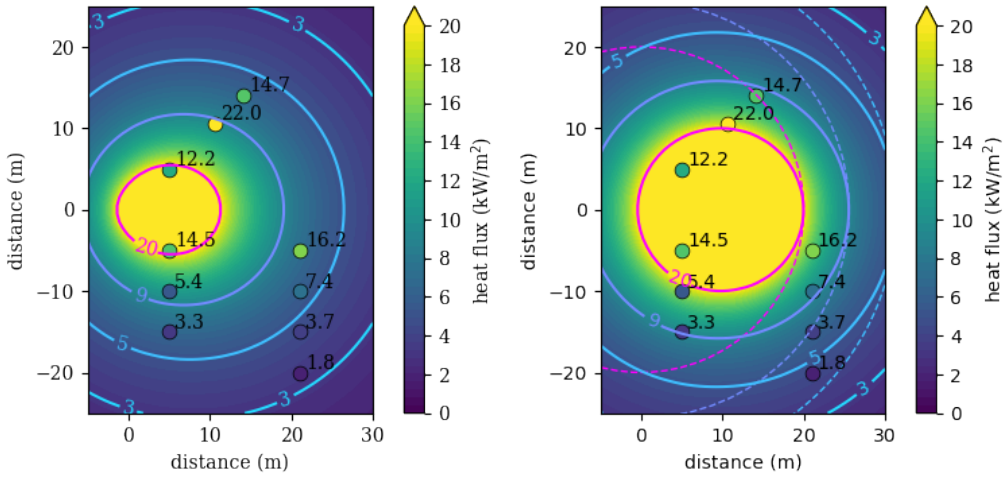


Figure 10. HyRAM+ heat flux predictions (shading and solid contour lines) vs data (points) for the DNV-GL test 6 flame [9], with the left-hand plot showing the predicted heat flux at the sensor height (1.2 m), and the right-hand plot showing the bird's eye view predicted heat flux.

3.4. Unconfined Overpressure

Pressure sensors were also present for the horizontal, ignited release during the DNV-GL experimental campaign, test 6 [9]. At the time of ignition, all of the pressure sensors peaked for about 0.1 seconds. One sensor reached 30 mbar while the others peaked about 10-20 mbar. The peak observed overpressures, as well as those overpressures predicted by HyRAM+ are shown in Figure 11. The HyRAM+ predictions use the Baker-Strehlow-Tang (BST) method as described in Ehrhart and Hecht [4], with modifications suggested by Jallais et al. [7] of using the flammable mass from 10-75%, and a Mach flame speed based on the mass flow rate (0.7 for this test). This is the same calculation as would be made during setback distance calculation. HyRAM+ vastly overpredicts the overpressures in this case. For context, the 207 mbar (3 psi) contour is also shown on the plot. This would be the overpressure-based setback distance for Group 3 hazards (discussed later).

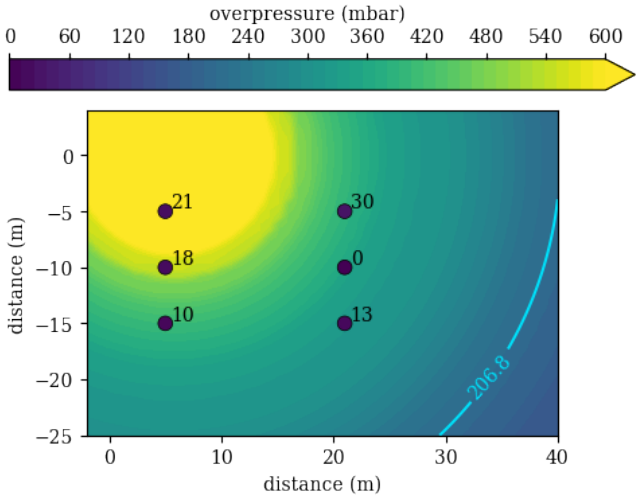


Figure 11. Peak overpressures observed after ignition of DNV-GL's test 6 (points) [9] as well as those predicted by HyRAM+ (shading and contour line).

3.5. Summary of Model Selection and Comparison

The algorithm for the homogeneous equilibrium model (HEM) for flow through an orifice was updated for version 4.1 of HyRAM+ to search for a maximum mass flux rather than rely on the uncertain 2-phase speed of sound calculation. For liquid hydrogen flows, this implementation agrees with other model predictions using a HEM. The flow rates predicted by the HEM tend to be equal to or larger than those measured experimentally. Notably this approach does not account for increased resistance from pipe wall frictions. The models for unignited dispersion from liquid hydrogen sources were compared to two data sets. The influence of wind was clear in the data, nonetheless, the streamline distance to an 8% mole fraction gives an accurate or slightly conservative estimate of where 8% mole fractions were observed in experiments. There was only a single set of heat-flux data from a liquid hydrogen flame that was compared to the HyRAM+ model. Again, some variability in the wind direction was evident in the data, but the birds-eye-view distances to different heat fluxes were conservatively predicted. Finally, the unconfined overpressure model was also compared to a single set of liquid hydrogen experiments. The overpressures were greatly overpredicted by the model, resulting in conservative distance predictions to overpressure values. In short, the separation distances calculated by HyRAM+ result in accurate or conservative predictions, albeit with limited liquid hydrogen data for validation.

4. HARM CRITERIA SELECTION AND JUSTIFICATION

The hazards associated with liquid hydrogen are similar to those associated with highly compressed gaseous hydrogen. With its low saturation temperature, a liquid leak will generally flash to vapor due to the heat in the air as it mixes. Heat transfer from an ambient temperature surface will also cause the liquid to vaporize. Rain-out and pooling is possible, but only for very large flowrates or long contact time [8, 17, 18]. Once the fuel is in vapor form, it will still be cold, yielding a cryogenic hazard (e.g., the cold can freeze skin or embrittle normally flexible materials such as O-rings), but otherwise poses the same hazards as a leak from a compressed gaseous system stemming from the fact that the fuel could ignite. The plume itself could ignite, or ignition could occur after accumulation within an enclosure, so the extent to which the flammable concentration of an unignited plume extends is an important consideration. Even without accumulating in an enclosure, if the release does not immediately ignite, there can be overpressure generated from a delayed ignition of a release. Whether the release ignites immediately or is a delayed process, a cryogenic hydrogen jet flame will radiate heat, which also poses a risk to humans and structures.

Since the hazards associated with liquid hydrogen are similar to the hazards from gaseous hydrogen, it is logical to group the exposures from bulk liquid hydrogen in the same manner as gaseous separation distances. Table 7.3.2.3.1.1(A) in the 2020 Edition of NFPA 2 gives bulk outdoor gaseous hydrogen separation distances, and explanatory Annex sections give the rationale and justification for how those distances were determined [1]. In this analysis, updated exposure distances for liquid hydrogen are calculated for each of the 3 groups, rather than a distance for each exposure.

4.1. Unignited Concentration

Hazards from an unignited plume of hydrogen are primarily focused on prevention of accumulation, human effects, or ignition. In order to prevent accumulation of hydrogen in enclosures, the flammable cloud of hydrogen should not be able to reach building openings like doors and windows, nor air intakes such as for air compressors or ventilation systems. Additionally, sewer inlets should be considered for liquid hydrogen, as the flammable concentration could potentially enter underground sewers. Finally, people should be prevented from coming into contact with the flammable cloud, due to oxygen deficiency, potentially low temperatures of an unignited mixture, or the very high temperatures of a hydrogen fireball should the cloud ignite.

The NFPA Standard for the Production, Storage, and Handling of Liquefied Natural Gas (LNG) (NFPA 59A) provides fire protection, safety, and other requirements for LNG systems [19]. As LNG is also a cryogenic flammable gas, this standard can provide potentially useful comparisons for hazard criteria. Table 19.8.4.1.1 of the 2019 Edition of NFPA 59A notes the lower flammability limit as the consequence-based criteria for irreversible harm to and fatality of people within an ignited flammable gas cloud [19]. Originally, the gaseous hydrogen setback distances in NFPA 2 were also based on a concentration of 4% by volume lower flammability limit, but this was modified in subsequent code cycles. Currently, NFPA 2 uses a concentration of 8% by volume for determination of gaseous hydrogen setback distances, based on the ability to sustain ignition [1, 20, 21, 22]. Based on this determination of the ability to sustain ignition, the Group 1 exposure criterion for unignited concentration is 8% by volume. Since this hazard only considers the flammability of the cloud for air intakes and people (i.e., the lot line), no concentration criterion is used for the other exposure groups.

4.2. Jet Fire Heat Flux

Heat flux from a jet fire could harm or cause fatalities to people and/or damage structures. It is important to consider the exposure time for a given level of heat flux; heat flux levels that can be painful for short exposures could be fatal for long exposures. Different types of exposures are also important to consider, as people, cars, buildings, and combustibles all respond differently to a given level of heat flux.

For Group 1 exposures, there should be little damage to structures and negligible risk to people. This can include people and buildings at the lot line, which are therefore not part of, nor benefit from, the installation under consideration. Table 19.8.4.2.1 of the 2019 Edition of NFPA 59A gives a limit of 5 kW/m^2 heat flux for irreversible harm to people outdoors without any sort of protective equipment [19]. Originally, NFPA 2 used a 1.6 kW/m^2 criterion, based on an exposure at the property line [1]; this is consistent with other works that give a 1.6 kW/m^2 criterion for no harm for long exposures [23]. However, some prior editions of NFPA 2 modified this criterion for Group 1 exposures to use 4.7 kW/m^2, based on an exposure for an employee for 3 minutes, as the previous no-harm criterion was deemed to be overly conservative [1]. This level is consistent with other work that gives a limit of 4-5 kW/m^2 for pain and first degree burn for a 20 second exposure [23]. Based on these comparisons, this analysis uses 4.732 kW/m^2 as the heat flux criterion for Group 1 exposures.

For Group 2 exposures, fatalities should be prevented for people within the site itself. Table 19.8.4.2.1 of the 2019 Edition of NFPA 59A gives a limit of 9 kW/m^2 based on the fatality of a person outdoors without protective equipment [19]. The 2020 Edition of NFPA 2 gives a heat flux limit of 4.732 kW/m^2 based on the exposure of a person for 3 minutes [1]. Other work has noted a second degree burn after 20 seconds of exposure to a 9.5 kW/m^2 heat flux, and 1% lethality after 1 minute of exposure to 12.5-15 kW/m^2 heat flux [23]. Based on the possibility for serious harm and potentially death after moderate exposure times, the Group 2 criterion for heat flux is 9 kW/m^2.

Finally, for Group 3 exposures, the primary consideration is fire spread through the ignition of nearby materials. Table 19.8.4.2.1 of the 2019 Edition of NFPA 59A gives criteria of 25 and 30 kW/m^2 based on harm/fatality to a person inside a building with a combustible and non-combustible exterior, respectively [19]; this is based on the building catching fire and harming people inside. The 2020 Edition of NFPA 2 gives Group 3 heat flux criteria of 20 and 25.237 kW/m^2 for combustibles and non-combustibles, respectively, for gaseous hydrogen setback distances [1]. Based on these criteria, Group 3 exposures use a 20 kW/m^2 heat flux criterion in this analysis.

Ignition of nearby materials can occur more quickly when in direct contact with a flame. The 2020 Edition of NFPA 2 uses the visible flame length of a jet fire as another criterion for Group 3 exposures. Therefore, this analysis also uses visible flame length as a criterion for Group 3 exposures.

4.3. Peak Overpressure

Delayed ignition of flammable clouds, even in open/unconfined spaces, can still lead to harm to people and structures. This is usually measured in the peak overpressure experienced at the onset of a blast wave. Overpressure criteria are not considered in the 2020 Edition of NFPA 2 for gaseous hydrogen setback distances [1] but could be considered for future code revisions.

At the Group 1 exposure distance, there should be little damage to other structures and low risk to people. A person could be knocked over with approximately 7 kPa (1 psi) [7]. Glass windows in

buildings can break at very low peak overpressures; more significant damage can occur to houses at approximately 7 kPa (1 psi) [24, 25]. Table 19.8.4.3.1 of the 2019 Edition of NFPA 59A gives a 1 psi peak overpressure limit due to irreversible harm to a person outdoors, and the same limit for buildings [19]. Based on these comparisons, the Group 1 overpressure value is selected to be 1 psi (7 kPa).

At the Group 2 exposure distance, people may have a risk of injury, but fatality is unlikely. At 16 kPa (2.3 psi), there is some risk of eardrum rupture [23], the possibility of people being projected against obstacles [23], but very little (< 1%) probability of fatality [26]. Additionally, this level of overpressure can lead to the partial collapse of unreinforced walls [24, 25, 27, 28]. The Group 2 peak overpressure criterion is therefore selected to be 2 psi (13.7 kPa) for this analysis.

Finally, the Group 3 exposure distance is meant to prevent fatalities in people and significant damage to buildings. At 17 kPa (2.5 psi), there is a 1% chance of fatality, although other sources note lower probabilities for fatalities in the open [26]. Table 19.8.4.3.1 of the 2019 Edition of NFPA 59A gives a 3 psi limit for fatalities of people outdoors [19]. Serious structural damage can occur at these overpressure values, including collapse of unreinforced concrete or cinderblock walls (15-20 kPa or 2.2-2.9 psi) [23] and distortion of steel frame buildings (20.7 kPa or 3 psi) [25]. Based on these comparisons, the peak overpressure criterion for Group 3 exposures is 3 psi (20.7 kPa).

4.4. Summary of Harm Criteria

The hazardous criteria described above for each of the three exposure groups are:

- Group 1:
  - Average mole fraction of 8%
  - Heat flux of 4.732 kW/m^2
  - Peak overpressure of 1 psi (6.9 kPa)
- Group 2:
  - Heat flux of 9 kW/m^2
  - Peak overpressure of 2 psi (13.7 kPa)
- Group 3:
  - Heat flux of 20 kW/m^2
  - Visible flame length
  - Peak overpressure of 3 psi (20.7 kPa)

Distances to each of the given criteria are estimated, and the furthest distance selected within each exposure group.

This page left blank

5. SETBACK DISTANCE CALCULATIONS

Previous sections of this report have described the approach, basis, models, and criteria that were used for the calculation of setback distances. This section describes the calculations themselves, along with the resulting table values.

5.1. Calculation Method

The setback distances considered in this analysis are consequence-based distances to a given level of harm. In order to calculate these distances, a leak was specified based on a fixed circular orifice with a diameter calculated from the fractional pipe area of 5% (see Section 2), assuming the source of the hydrogen that flows through the orifice is saturated liquid hydrogen, and by using one of 3 different pressures. Each of these pressures represents a bin of pressure ranges, as specified in Table 5. For pressures up to 929 kPa (120 psi), the highest value in the pressure range is used to calculate the distance, as this will give the longest unignited plume, longest jet flame, largest distance to a specific radiation contour, or the largest flammable mass and subsequent overpressure for the pressure range. For the highest pressure range, which is valid for pressures up to the critical pressure for hydrogen (1.20 MPa or 173 psi, otherwise this would not be a liquid hydrogen storage system), the pressure value of 1,091 kPa (158 psi) is used as this pressure will give the maximum mass flux and longest distance. Saturated liquid at pressures above 1,091 kPa (158 psi) will have lower mass fluxes and shorter distances. In this way, each of the pressure values gives the longest distance for each range given. The pressures are given in gauge pressure assuming at ambient pressure of 1 atm (101.325 kPa). The leak is then assumed to be steady-state, and various potential hazards are calculated based on the unignited plume or jet fire.

Table 5: Representative pressure values used for each pressure range in calculation of setback distances

Pressure Range	Pressure Value Used
≤414 kPa (≤60 psi)	414 kPa (60 psi)
414< $P \leq$ 827 kPa (60 < $P \leq$ 120 psi)	827 kPa (120 psi)
827 < $P \leq$ 1200 kPa (120 < $P \leq$ 173 psi)	1,091 kPa (158 psi)

The HyRAM+ model for unignited dispersion is a one-dimensional conservation of mass, momentum, species, and energy along the streamline [4]. This streamline can curve due to the buoyancy of the fluid being transported. This can become important for low-speed hydrogen flows due to the low density of hydrogen. While cryogenic hydrogen is much denser than warm hydrogen, it becomes buoyant just above the saturation temperature. The liquid hydrogen will vaporize before mixing and dispersing with the air. An example unignited plume is shown in Figure 12. The 4% by volume contour (mole fraction of 0.04) demonstrates the buoyancy of the hydrogen/air mixture, even though the source of the hydrogen is saturated liquid. The 8% by volume (mole fraction of 0.08) shows less of an obvious buoyancy effect, but still trends upward slightly. The distance of interest is the distance along the streamline to the unignited concentration of 8% by volume; in Figure 12 this is 13.3 m. This streamline distance is conservative due to this buoyancy, because the streamline distance follows the path of the plume, but for the purposes of the setback distance is assumed to be a straight horizontal distance. This streamline distance for unignited dispersion also does not take wind into account; this is also conservative due to the fact that the releases are already largely horizontal and that wind in any direction tends to disperse hydrogen rather than extend the flammable range [13].

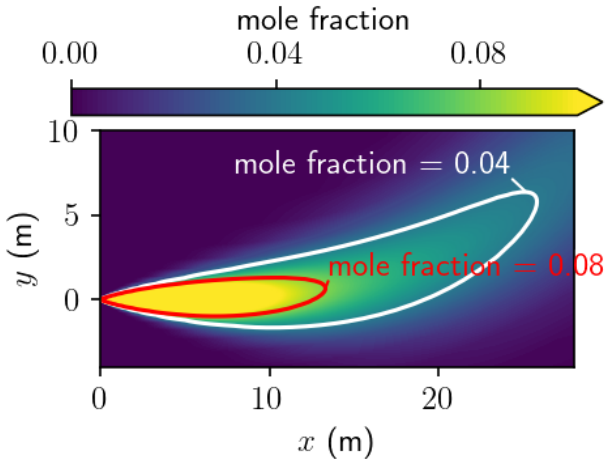


Figure 12: Unignited concentration plume from a steady-state saturated liquid hydrogen leak through an 8.5 mm (0.3 in) circular orifice (5% leak area of a 38 mm [1.5 in] pipe) at 414 kPa (60 psi) gauge pressure

Similar to the dispersion model, the jet flame model in HyRAM+ is also a 1-dimensional system of ordinary differential equations with a single dependent spatial variable along the streamline [4]. This model also predicts the curvature of a flame due to buoyancy. The trajectory and heat flux contours for the highest-momentum jet flame considered are shown in Figure 13. The flame shown by the black line in the figure clearly bends upwards due to buoyancy, even with a 5 m/s horizontal wind affecting the momentum. This wind speed only affects the jet flame momentum in the horizontal direction; it does not help to disperse heat or offer any other beneficial effects. It should be noted that this wind momentum capability was added to the back-end (Python-only) version of HyRAM+ 4.1; it is not accessible through the front-end graphical user interface. Because these flames are predicted to be so buoyant, considering the flame length and heat flux values along the streamline of the flame would lead to unrealistically large exposure distances. Therefore, exposure distances to both the flame length and the different heat flux contours are based on the overhead projection of the flame trajectory and heat flux contours (i.e., the lower left frame in Figure 13). This contour and flame length is assessed at the height of the flame centerline at ¾ of the total flame length, as this is the point along a flame that radiation tends to peak [29]. For the flame shown in Figure 13 the birds-eye-view visible flame length is 8.84 m, and the distance to the 9 kW/m^2 heat flux contour is 11.64 m.

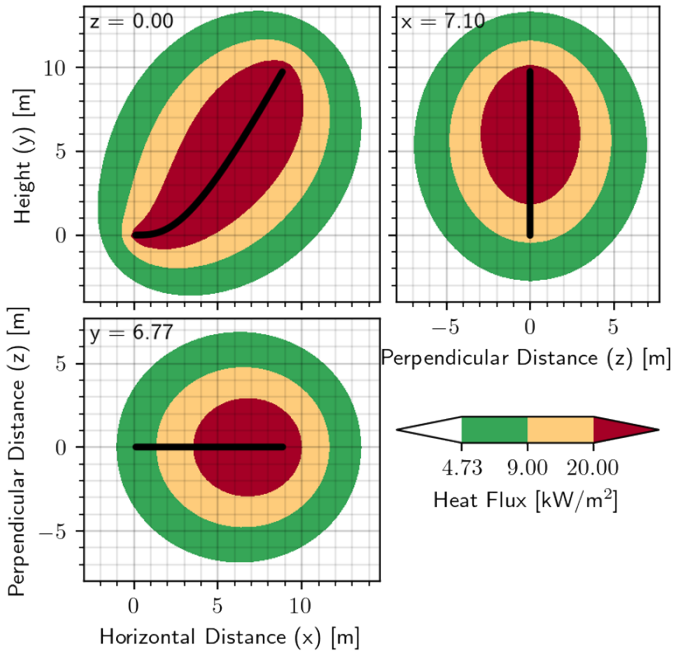


Figure 13: Jet flame heat flux contours for an ignited, steady-state, saturated liquid hydrogen leak through an 8.5 mm (0.3 in) diameter (5% leak area of a 38 mm [1.5 in] pipe) circular orifice at 1,091 kPa (158 psi) gauge pressure, with 0.9 relative humidity and a horizontal wind speed of 5 m/s. The black line shows the jet flame streamline up to the visible flame length. The top-left plot shows a side-on view, the top-right plot shows an end-on view, and the bottom-left plot shows a top view.

Unconfined overpressure in HyRAM+ is estimated based on the flammable mass within a steady-state unignited jet plume [4]. The Baker-Strehlow-Tang (BST) method is used to estimate the peak overpressure at different distances away from the overpressure origin. The overpressure origin is assumed to be the point along the jet streamline coordinate at which the concentration is halfway between the upper and lower flammability limits; for hydrogen, this concentration is 39.5% by volume. The entire flammable mass of hydrogen in an unignited plume would use the full range of flammability limits between 4% and 75% by volume, which can be calculated by volumetrically integrating the product of the mass fraction and density of the jet/plume that is within the flammability limits. However, according to the work of Jallais et al. [7] the results are more accurate for unconfined overpressures if the lower concentration limit is 10% by volume instead of 4% by volume. Jallais et al. [7] also recommend that the blast wave curve be selected based on the leak flow rate; for the example in Figure 14 the mass flow rate of 0.16 kg/s leads to the 0.35 Mach flame speed curve for the BST method. The distance of interest is then the maximum horizontal distance from the leak point shown as the black dot in the figure (not the overpressure origin) to the peak overpressure value of interest, i.e., in the positive x-direction. For the example shown in Figure 14, the distance to a peak overpressure of 13.79 kPa (2 psi) is 6.78 m. Note that pressure reflections from walls or equipment are not accounted for within this implementation, although reflection of the blast wave off the ground is accounted for in the BST model.

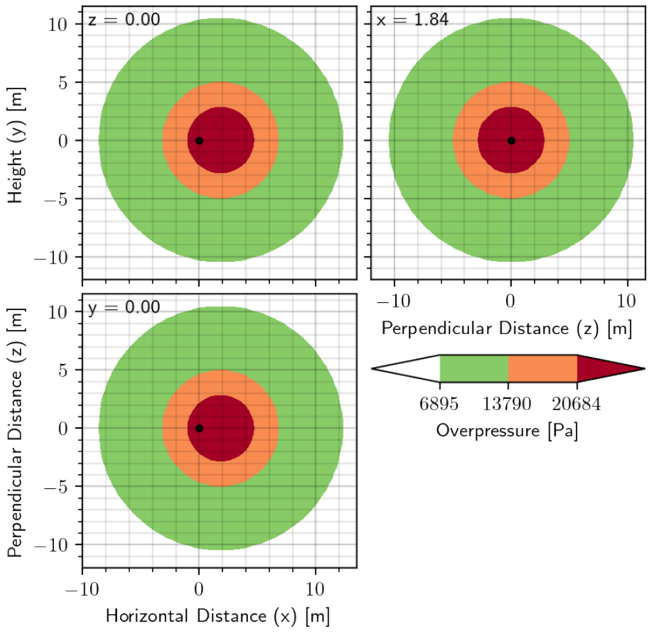


Figure 14: Unconfined overpressure resulting from delayed ignition of a steady-state saturated liquid hydrogen leak through an 8.5 mm (0.3 in) circular orifice (5% leak area of a 38 mm [1.5 in] pipe) at 414 kPa (60 psi) gauge pressure. The top-left plot shows a side-on view, the top-right plot shows a side-on view, the top-right plot shows an end-on view, and the bottom-left plot shows a top view.

Once distances have been calculated for each of the hazard metrics of interest for each exposure group, the maximum distance (e.g., distance to the heat flux metric or the distance to the overpressure metric) is then selected within each exposure group. Thus, while all hazard metrics are considered through the calculation of distances, the longest distance within each group determines the setback distance for that exposure group for each pipe diameter and pressure. These values are tabulated such that there is a distance for a pipe diameter for each pressure group. In addition, a linear fit is calculated to relate distance to the pipe diameter for each pressure group and the fitted line is included as an alternative means of calculating a distance for alternative pipe diameters without interpolating. It should be noted that the gaseous hydrogen setback distances used a safety factor of 50% (1.5) on the final setback distances [1] however, the more conservative leak size assumptions used in this analysis eliminates the need for a safety factor.

5.2. Exposure Group Setback Distance Calculations

Setback distances for the hazard criteria in exposure Group 1 are shown in Figure 15. As shown in the figure, distances are estimated for each of the different hazard criteria and each of the pressures of interest. Within each pressure range, the largest distance is selected as the final setback distance. A thick line for each pressure range shows this maximum distance. A dashed line (mostly overlapping the thick line) for each pressure range shows the linear fit. For Group 1, the distance to the 8% by volume unignited concentration drives the final setback distances. Note that this plot shows the inner pipe diameter on the horizontal axis, but the calculations use 5% of the flow area for that pipe diameter as the leak size in the calculation of distance.

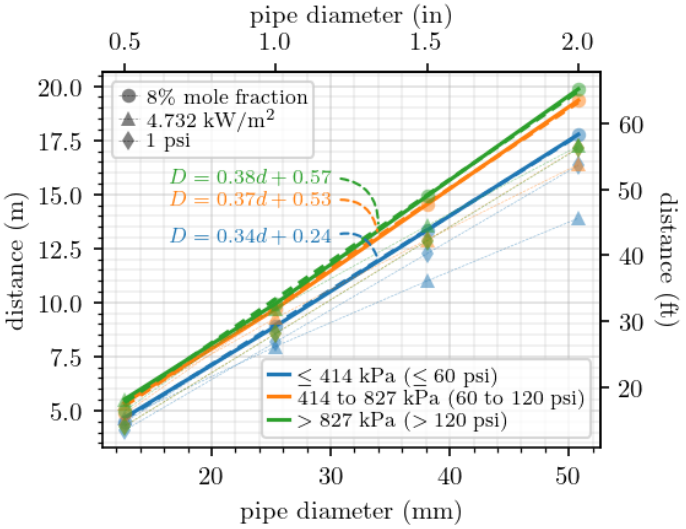


Figure 15: Setback distances for exposure Group 1

Setback distances for the hazard criteria in exposure Group 2 are shown in Figure 16. The thick line for each color group shows the maximum distance within each pressure range. For Group 2, the distance to the 9 kW/m² heat flux drives the final setback distances.

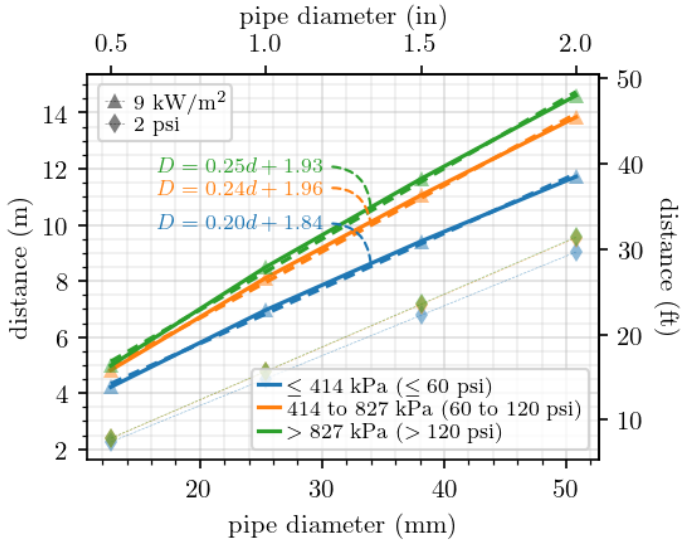


Figure 16: Setback distances for exposure Group 2

Setback distances for the hazard criteria in exposure Group 3 are shown in Figure 17. The thick line for each color group shows the maximum distance within each pressure range. For Group 3, the distance to the 20 kW/m² heat flux drives the final setback distances.

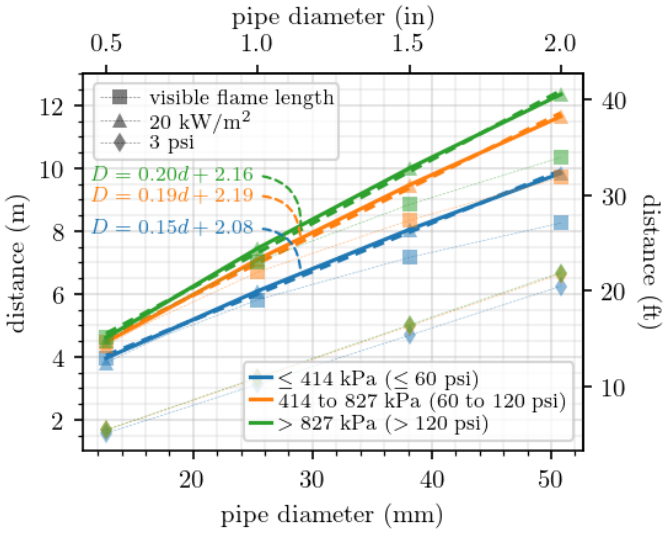


Figure 17: Setback distances for exposure Group 3

5.3. Resulting Setback Distance Calculation Tables

Two tables were created for inclusion in NFPA 2. The first table is shown in Table 6 and gives the minimum setback distances for outdoor bulk liquid hydrogen systems for a typical pipe with an inner diameter of 38.1 mm (1.5 in). The second table is shown in Table 7 and gives the same minimum setback distances but also varies the pipe inner diameter and includes the formulas based on the diameter.

Table 6: Minimum distance from outdoor bulk liquefied hydrogen systems to exposures for typical pipe inner Diameter 38.1 mm (1.5 in)

Maximum Tank Operating Pressure (gauge)	≤ 60 psi ≤ 414 kPa		60 to 120 psi 414–827 kPa		>120 psi >827 kPa	
Exposures Group 1	**m**	**ft**	**m**	**ft**	**m**	**ft**
1. Lot lines 2. Air intakes (e.g. HVAC, compressors) 3. Operable openings in buildings and structures 4. Ignition sources such as open flames and welding	13.3	44	14.5	48	14.9	49
Exposures Group 2	**m**	**ft**	**m**	**ft**	**m**	**ft**
5. Exposed persons other than those servicing the system 6. Parked cars 7. Buildings of combustible construction 8. Hazardous materials storage systems above ground or fill/vent openings for below ground storage systems 9. Ordinary combustibles, including fast-burning solids such as ordinary lumber, excelsior, paper, or combustible waste and vegetation other than that found in maintained landscaped areas	9.4	31	11.1	36	11.6	38
Exposures Group 3	**m**	**ft**	**m**	**ft**	**m**	**ft**
10. Buildings of noncombustible non-fire-rated construction 11. Flammable gas storage systems above or below ground 12. Heavy timber, coal, or other slow-burning combustible solids 13. Unopenable openings in buildings and structures 14. Encroachment by overhead utilities (horizontal distance from the vertical plane below the nearest overhead electrical wire of building service 15. Piping containing other hazardous materials 16. Flammable gas metering and regulating stations such as natural gas or propane	8.0	26	9.5	31	10.0	33

Table 7: Minimum distance from outdoor bulk liquefied hydrogen systems to exposure by maximum inner diameter

MOP (gauge)		≤ 414 kPa, ≤ 60 psi						414 to 827 kPa, 60 to 120 psi						> 827 kPa, > 120 psi					
		Group 1		Group 2		Group 3		Group 1		Group 2		Group 3		Group 1		Group 2		Group 3	
Inner Diameter		$0.34d + 0.24$		$0.20d + 1.84$		$0.15d + 2.08$		$0.37d + 0.53$		$0.24d + 1.96$		$0.19d + 2.19$		$0.38d + 0.57$		$0.25d + 1.93$		$0.20d + 2.16$	
in	**mm**	**m**	**ft**	**m**	**ft**	**m**	**ft**	**m**	**ft**	**m**	**ft**	**m**	**ft**	**m**	**ft**	**m**	**ft**	**m**	**ft**
1/2	12.7	4.7	15	4.2	14	4.0	13	5.4	18	4.8	16	4.5	15	5.5	18	5.0	16	4.6	15
1	25.4	8.9	29	7.0	23	6.1	20	9.7	32	8.1	27	7.1	23	10.0	33	8.5	28	7.5	24
1 1/2	**38.1**	**13.3**	**44**	**9.4**	**31**	**8.0**	**26**	**14.5**	**48**	**11.1**	**36**	**9.5**	**31**	**14.9**	**49**	**11.6**	**38**	**10.0**	**33**
2	50.6	17.8	58	11.7	38	9.8	32	19.3	63	13.8	45	11.6	38	19.9	65	14.6	48	12.3	41

Note: Fitted equations yield distance in meters using inner diameter "d" in mm

This page left blank

6. MITIGATIONS JUSTIFICATION

The NFPA 2 code has previously allowed for reductions to setback distances based on specific and well-defined mitigations that can reduce the risk and thereby decrease the separation distance that must be met. The same approach is considered here, and both passive (in which no action is needed) and active (in which an action is taken in response to a leak) mitigations are considered.

6.1. Passive Mitigations: Walls

The justification for use of walls as a passive mitigation measure for liquid hydrogen storage is leveraged from work previously completed for gaseous hydrogen releases. This was deemed applicable to liquid hydrogen storage due to any released hydrogen quickly vaporizing. As such, liquid hydrogen leaks pose similar hazards as the gaseous leaks previously considered (flammable vapors, heat flux from flames, and overpressure from ignition). The previous work studied the effectiveness of barrier walls to reduce hazards using both experimental and modeling efforts [30]. Risk based distance reductions based on those experimental and modeling efforts were then proposed by LaChance et al. [31] and informed revisions to NFPA 2 gaseous hydrogen storage setback distances [32].

Schefer et al. [33] completed a series of experiments where fixed quantities of hydrogen were released and ignited, with the resulting jet flame directed towards a variety of barrier wall geometries. The resulting heat flux and overpressures at spatial locations within and beyond the barrier walls were measured, providing a quantitative characterization of walls' hazard mitigation effectiveness. Through this set of experiments, it was found that the walls were effective in reducing heat flux and overpressures beyond the wall. Another important finding was that entrainment of hot combustion gases down the backside of the walls was not observed.

A complementary modeling effort by Houf et al. [30] further investigated the impact of barrier walls on heat flux and overpressures from ignited jet flames as well as concentration envelops from unignited flows. Computational fluid dynamics and radiation transport simulations were used in the modeling effort after being validated against experimental data from the previous effort. The model predictions supported the experimental findings that wall barriers could significantly reduce heat flux and overpressure hazards beyond the wall and also found that barrier walls were effective at reducing hydrogen concentrations beyond the wall by containing and deflecting it upwards.

LaChance et al. [31] used the experimental and modeling results as an evidence basis for suggesting reduced setback distances for gaseous hydrogen storage applications, based on the resulting reduction in risk posed to the public outside of the barrier walls. The QRA methodology previously developed for general gaseous hydrogen setback distances [4] was used to predict risk for a scenario with barrier walls. Risk reductions are based on proper wall design and construction, where barrier walls must block the line-of-site to the exposers in order to block leak consequences. The consequence due to direct contact with a resulting jet fire is removed by placing a wall between the public and leak. Based on the reductions to heat flux and overpressure, individual risks were calculated for the setback distances suggested at the time, and distances were calculated at which the accepted risk value was met with the barrier wall limited heat flux calculations. These risk-based distance findings ultimately informed a mitigation credit in the 2011 edition of NFPA 2, which was a 50% setback distance reduction for gaseous hydrogen storage systems with barrier walls [32]. It should be noted that the risk analysis actually supported a reduction by as much as 66%, but the NFPA 2 Hydrogen Technologies Technical Committee ultimately decided that a 50% reduction was more conservative. However, this reduction was based directly on a risk-based distance, while the

setback distances themselves were consequence-based; more information about the use of walls to reduce the physical hazards directly could better inform future reductions to setback distances based on walls. It should be noted that while a wall mitigates heat flux beyond the wall, the potential for increased heat to equipment that remains inside the walled area should not be ignored.

6.2. Active Mitigations: Automatic Shutoff Valve

Another way to potentially reduce the risk or hazards from a liquid hydrogen leak would be to have an active system that automatically shuts off the supply of hydrogen once a leak is detected. This could reduce the extent of a flammable cloud, enable dispersion of the hydrogen before it has time to ignite, or simply reduce the total amount of hydrogen released; all of these can reduce potential hazards and thereby the risk to nearby people and buildings. Various potential benefits to an automatic shutoff valve are considered for potential reductions to setback distances.

6.2.1. Heat Flux Exposure Time

The harm from heat flux can be quantified in terms of a thermal dose unit (V), which includes both the heat flux value itself (I) as well as the exposure time (t) as shown in Equation 1 [4].

$$V = I^{(4/3)} \times t \qquad \text{Equation 1}$$

The thermal dose unit can then be used with various fatality models to estimate the probability of a fatality; in this case, the Tsao & Perry probit model was used as implemented in HyRAM+ version 4.1 [4]. Using these models, the probability of a fatality for various heat flux values and various exposure times was calculated. Figure 18 shows the fatality probability as a function of heat flux for various exposure times. The 2020 edition of NFPA 2 uses a heat flux value of 4.732 kW/m^2 for gaseous hydrogen Group 1 exposures, based on a 3-minute exposure time [1]; this results in an 80% probability of fatality as shown by the brown curve in Figure 18. However, if the proposed heat flux criterion of 9 kw/m^2 is used along with a more realistic exposure time of 30-60 seconds (see Section 4.2 for discussion), then the probability of a fatality is 6-60% (where the red and purple curves intersect with the vertical black line at 9 kW/m^2), even lower than the fatality probability that results from the 2020 edition NFPA 2 gaseous hydrogen criterion.

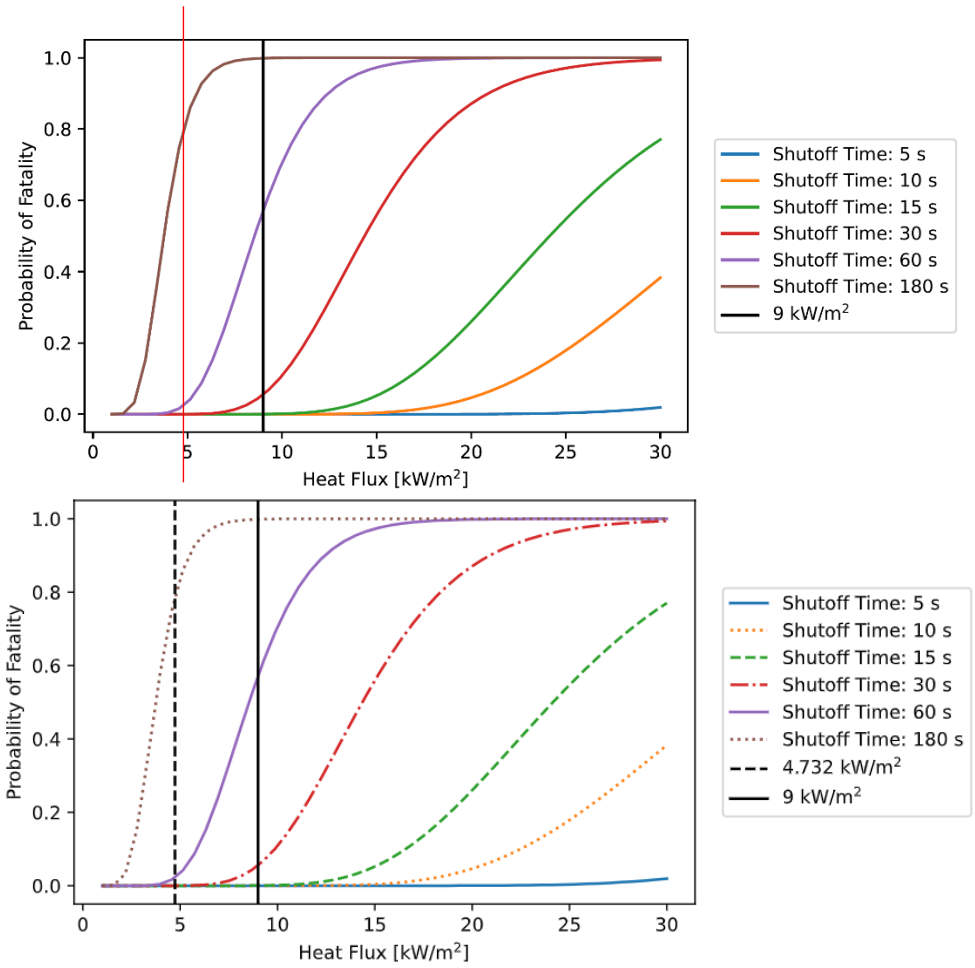


Figure 18: Probability of fatality at different heat flux values for different exposure times

If an automatic shutoff valve could decrease the exposure time even more, this could reduce the probability of a fatality even further. If an automatic shutoff valve could be shown to reduce the leak duration to 15 seconds, this would reduce the probability of fatality to 0% at the proposed higher heat flux value of 9 kW/m². It is important to note, however, that even if the detection of the flame and activation of the automatic shutoff valve could occur within 15 seconds, that may not immediately result in the flame stopping; depending on where the leak occurred, there may be significant quantity of hydrogen in between the shutoff valve and the leak point, which could lead to a fire continuing for some time after the shutoff valve has been activated.

6.2.2. Time to Ignition

Another potential mitigation provided by an automatic shutoff valve is the prevention of fire spread to nearby buildings or structures, which causes additional damage and safety hazards. One way to quantify this effect is to consider the time it would take for various building materials to ignite; if the materials don't ignite, the fire doesn't spread. The relationship between time to ignition and heat flux for various building materials [34] is shown in Figure 19. The 20 kW/m² heat flux value is used for Group 3 combustible exposures for bulk gaseous hydrogen storage in NFPA 2 2020 Edition [1] and is proposed for use with liquid hydrogen Group 3 exposures.

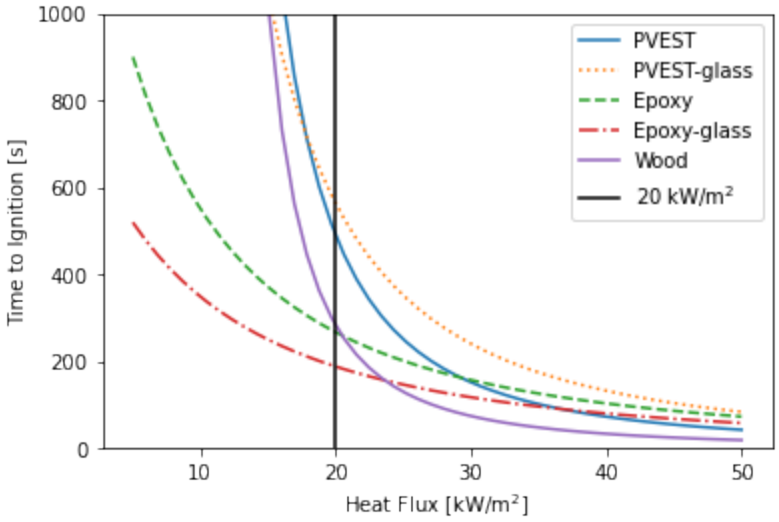


Figure 19: Time to ignition for different building materials (using values from [34])

As shown in Figure 19, at 20 kW/m² heat flux, it would take all of the relevant building materials approximately 200 seconds (3.3 minutes) or more to ignite. This suggests that if an automatic shutoff valve could stop an ignited hydrogen leak within that time, fire propagation to other structures would not occur. This suggests that Group 3 distances could be reduced by the use of an automatic shutoff valve; however, the effect of jet fires on humans would also need to be considered. Figure 18 shows that for 20 kW/m² (the heat flux criteria for Group 3 exposures), the probability of fatality can be significant for all but very shortest exposure times (5-10 seconds). However, since Group 3 exposures apply to people servicing the system, it could be that maintenance staff would be wearing protective clothing, which could significantly alter the fatality probabilities shown in Figure 18. This implies that a very fast-response automatic shutoff system could be used for Group 3 reductions, potentially in combination with requirements to use protective clothing.

6.2.3. Ignition Probability

Another potential benefit for an automatic shutoff valve is the reduction in likelihood of ignition. A shorter duration leak may have less opportunity to encounter an ignition source; some analyses in the literature (e.g., [35]) have developed a probability of ignition over time based on the expanding volume of the flammable cloud. This assumes that the flammable cloud continues to expand, and that the flammable cloud expands over areas that have a particular ignition probability. However, it is not clear that this model is directly applicable to hydrogen releases. Hydrogen releases, even liquid hydrogen releases, tend to dissipate quickly after release and reach a steady state, not an ever-expanding flammable cloud. Furthermore, hydrogen is more easily ignited than most hydrocarbons, including a self-ignition mechanism in which a distinct external ignition source may not be needed. Even so, an automatic shutoff valve that results in a shorter duration leak can still reduce the probability of ignition, as it would still presumably reduce the chance of encountering an ignition source or for self-ignition to occur. Unfortunately, it is not immediately clear how this benefit should be quantified, and therefore not clear how much reduction benefit should be given for setback distances.

6.3. Summary and Conclusions

Walls are a straightforward passive mitigation that provide a direct barrier between a hazard and a potential person or building. Prior analyses have suggested that walls can reduce risk and thereby can reduce the setback distances. These same reductions would certainly still apply for bulk liquid hydrogen storage systems, given the similarities between the prior gaseous hydrogen setback distance calculations and the current work. However, more information specific to liquid hydrogen could be useful in better refining the potential distance reduction that walls can provide.

There are a number of potential ways in which the benefit of an automatic shutoff valve could be quantified. However, these methods tend to focus on specific hazards such as heat flux from a jet flame, and do not consider other hazards, such as the unignited flammable cloud extent, nor overpressure hazards from a delayed ignition. These other hazards could be quantified in the future, and if so, could lead to a clear and defensible reduction in setback distances for hydrogen releases. At this point, it is not clear how to quantify the benefit to hazard reduction for all the relevant hazards considered for setback distance calculation.

However, it is important to consider that some bulk liquid hydrogen storage occurs at public refueling retail sites. Unlike more isolated industrial sites, there are many more untrained people and uncontrolled activities in the area surrounding a bulk liquid hydrogen storage tank, even if access to the storage tank itself is still controlled. Therefore, it may be worth requiring an automatic shutoff valve for bulk liquid hydrogen storage tanks in public refueling facilities to reduce the overall risk, given the expected increase in risk due to the presence of untrained individuals and uncontrolled activities. To be clear, this would not confer a reduction in setback distances, but would simply be an additional requirement for bulk liquid hydrogen storage tanks at public refueling facilities. With better quantification of the increased risk at public refueling facilities and decreased risk due to an automatic shutoff valve, this requirement could be refined in the future.

This page left blank

7. SUMMARY AND CONCLUSIONS

7.1. Summary

Setback distances define a prescribed distance between a potentially hazardous system and different types of other systems, people, buildings, or materials that may be exposed to that hazard. A task group of the NFPA 2 Hydrogen Technology Technical Committee reviewed the previous liquid hydrogen setback distances. Similar to prior revisions for bulk gaseous hydrogen setback distances, a leak size was chosen that was informed by quantitative risk assessment; this leak size serves as a proxy for those more detailed and variable risk assessments and allows consequence-based distances to be calculated for a specific leak size based on selected physical criteria. Similar to the bulk gaseous hydrogen setback distance tables, exposures were grouped into exposure groups, and applicable physical harm criteria were chosen for each exposure group. Finally (and again similar to the bulk gaseous hydrogen setback distance table), setback distances were calculated for bulk liquid hydrogen storage based on the chosen leak size and to the chosen harm criteria and were related to pipe size and system pressures, rather than the quantity of liquid hydrogen stored.

The risk-informed basis for leak size began with a risk analysis for a representative liquid hydrogen storage system, resulting in the distance at which a specified risk metric was met. Equivalent leak hole sizes were then calculated that would result in the same distance to physical criteria for concentration, heat-flux, and maximum overpressure as the risk-based distance. These equivalent hole sizes were then normalized by the cross-sectional flow area of the pipe. A sensitivity study was then used to demonstrate the impact of varying inputs and assumptions to the risk assessment. This sensitivity study resulted in the selection of a 5% fractional hole size as being a conservative, but not unrealistic, basis for liquid hydrogen storage system setback distances. This leak size was compared to potential leak sizes from commercially-available liquid hydrogen bayonet connectors, and the 5% fractional leak size was again shown to be conservative.

The physical models were compared to data to ensure that they result in realistic predictions of cryogenic hydrogen dispersion, flames, and overpressure. The flow rates predicted by the HyRAM+ model tend to be equal to or greater than two experimental data sets. The models for unignited dispersion from liquid hydrogen sources were also compared to two data sets. The streamline distance to an 8% mole fraction was shown to be an accurate or slightly conservative estimate of the experimental observations. There was only a single set of heat-flux data from a liquid hydrogen flame that was compared to the HyRAM+ model, but the birds-eye view of the heat fluxes were shown to be conservative relative to the experimental measurements. Finally, the unconfined overpressure model was also compared to a single set of liquid hydrogen experiments; the overpressures were greatly overpredicted by the model, resulting in conservative distance predictions to overpressure values. In short, the separation distances calculated by HyRAM+ result in accurate or conservative predictions, albeit with limited liquid hydrogen data for validation.

Physical harm criteria are used with the hole size and physical release models to estimate the distance to a given level of hazard. Unignited concentrations, heat flux from a jet fire, visible flame length, and peak overpressure were all considered for the three exposure groups. Group 1 exposures include lot lines and air intakes, and should yield negligible risk to buildings or people. An 8% by volume unignited concentration was selected, based on the ability to sustain ignition, as well as a 4.732 kW/m^2 heat flux and 7 kPa (1 psi) peak overpressure. Group 2 exposures include exposed persons not servicing the system and parked cars, and should prevent fatalities for people on the site itself although there may be some risk of injury. A heat flux of 9 kW/m^2 was selected for Group 2 exposures, as well as a 13.7 kPa (2 psi) peak overpressure. Finally, Group 3 exposures should

prevent fatalities to people, significant damage to buildings, and prevent fire spread that would make an incident worse. A heat flux of 20 kW/m^2 was selected for Group 3 exposures, as was the visible flame length and a peak overpressure of 20.7 kPa (3 psi). Some of these criteria are similar to those used previously in NFPA 2 for gaseous hydrogen, although some have been updated and overpressure is now explicitly considered.

Using the selected leak size, the verified and validated models and the selected criteria, two tables of setback distances were developed, similar to the gaseous setback distance tables. One table shows the distances for each group of exposures, for three pressure ranges, for a typical pipe size, and the other relates the distances to both system operating pressure and pipe size. While the overall process for developing these distances was similar to and informed by the prior methodology for bulk gaseous hydrogen, there are some differences. One is the elimination of a 1.5 (50%) safety factor, that had been applied to the calculations of the bulk gaseous hydrogen setback distances when the leak size was reduced from 3% to 1%. A safety factor is inherent to this analysis due to the conservative 5% leak size and the conservative distances predicted by the models, much like the initial, conservative 3% leak size for bulk gaseous setback distances.

Mitigations to reduce the setback distances were also considered. Walls can provide a direct barrier between a hazard and a potential person or building. Prior analyses have suggested that walls can reduce risk and thereby can reduce the setback distances. These same reductions would certainly still apply here, given the similarities between the prior gaseous hydrogen setback distance revisions and the current work. There are a number of potential benefits to active mitigations like an automatic shutoff system. Quantifying the benefit of active mitigations is an area for future work. That said, it is important to consider that some bulk liquid hydrogen storage occurs at public refueling retail sites. Therefore, it may be worth requiring an automatic shutoff valve for bulk liquid hydrogen storage tanks in public refueling facilities to reduce the overall risk, even if there is no direct reduction in setback distances.

7.2. Technical Committee Criteria

This analysis was developed in close communication and collaboration with members of the NFPA 2 Technical Committee and Storage Task Group. As part of that process and during the NFPA 2 revision cycle, the Technical Committee outlined criteria that should be followed for a successful code revision. While these are not formal criteria for any code revision, we felt the criteria to be very useful and helped to inform this overall analysis and approach. Therefore, the committee criteria are outlined here along with notes of how this analysis addresses each point. The NFPA 2 Technical Committee suggested that the analysis methodology be well-documented, retrievable, repeatable, revisable, independently-verified, and use experimental results to verify and validate behavior models.

Well-Documented A well-documented analysis and calculations are critical for members of the committee, members of the public, and relevant stakeholders to understand how a requirement was determined. Well-documented analyses, calculations, and models form the basis for the criteria that follow. In this case, the analysis and results were presented multiple times to the NFPA 2 Storage Task Group and presented to the NFPA 2 Technical Committee prior to the formal committee meeting so that members of both groups had time to review the presentation materials, ask questions, and provide feedback. Additionally, an Annex to the NFPA 2 code was added with a clear and concise explanation of the process, the models used, the experimental results that were compared against the models, and how the resulting setback distances were calculated. This report is meant to be a more detailed account of the entire methodology, including justification for the leak

size basis, justification for the hazard criteria used for each exposure group, model specification and comparison to data, and the resulting setback distance values. Finally, the models used in the calculations described here are part of a free and open-source software which is publicly available for review.

Retrievable The documentation of the methodology and models used should be in an easily-accessible place for interested parties to be able to review. The explanation in the code annex will be part of the NFPA 2 document, meaning that anyone who has access to the document requirements will be able to read the explanatory annex. This report will be published without restriction and available on Sandia National Laboratories and Department of Energy websites for anyone to freely access. The models used are part of a free and open-source software (HyRAM+), which is available on a publicly-accessible website: https://hyram.sandia.gov.

Repeatable The calculations performed should be repeatable by third-parties in order to confirm the results and identify errors. The models and calculations used in this analysis are freely available and open source, meaning that anyone can use the Python programming language to repeat the calculations for themselves. The background and justification for the models are described here, meaning that anyone can also develop their own versions of the calculations used in order to repeat the calculations.

Revisable The methodology should be easily revisable, so that different decisions in the future can be made based on new information or different assumptions. This report aims to clearly identify the assumptions made and the sources of information considered. The well-documented, retrievable, and repeatable calculations described here mean that if new information is obtained or different assumptions are made in the future, this same methodology can be revised and re-done to obtain different results within the same overall framework. This is critical to enable continuous improvement and refinement of the requirements to better promote safe design, installation, and operation of liquid hydrogen systems.

Independently-Verified Independent verification is important to ensure that models are implemented as described, assumptions are reasonable, and results are similar. This report describes efforts through the NFPA 2 Storage Task Group to verify and compare results from Sandia to those obtained by Chart Industries and Air Products.

Experimental Verification of Models Numerical models can be based on sound scientific reasoning, but should be verified and validated against experimental results in order to check both the underlying model logic and implementation of the numerical methods. This report describes how currently available data from liquid hydrogen release experiments were used to verify and validate the models used in the calculation of setback distances.

7.3. Future Work

This document describes the process used and justification for revisions to bulk liquid hydrogen storage setback distances in NFPA 2. However, there are ways in which this analysis could be improved or modified in the future, and there are also ways in which this analysis (or something like it) could be applied to other requirements in NFPA 2 or elsewhere.

7.3.1. Incorporation of More and Better Data

First and perhaps most obviously, the physical release behavior models could be improved. This can be done through additional validation (for which there is currently a dearth of data) with different

release conditions, such as leak orifice sizes and shapes as well as storage pressures and temperatures. Some of the mass flow rate assumptions described in this report tend to be conservative, but are compared to very little data; additional experimental data for comparison and improvement of these models could reduce conservatisms. Additionally, this analysis does not explicitly consider pooling of large-scale liquid hydrogen releases. While it may be that the hazards from a liquid hydrogen pool may be effectively covered by the existing hazards (jet fire, etc.), this was not specifically considered and may not always be true. Finally, while unconfined overpressure effects were considered in this analysis, overpressure behavior is inherently complicated and could be improved in future analyses. For example, congestion of a hydrogen/air mixture due to tubing or pieces of equipment could lead to a more intense blast wave. Additionally, blast waves could reflect off of nearby walls, buildings, or other structures, leading to potentially higher overpressures in some situations. While some conservative assumptions can help account for this, considering these effects explicitly may still be useful in some cases.

Another area in which this analysis could be improved is the incorporation of more and better data for the leak frequency of liquid hydrogen components. While more and better data in general is always beneficial, in this case the leak frequencies used in the risk assessment were highly uncertain and informed by oil and gas industry, liquefied natural gas, and gaseous hydrogen data, rather than liquid hydrogen specifically. Furthermore, anecdotal conversations with some industry experts have indicated that most liquid hydrogen system leaks occur at the transfer point when a tanker is being filled or emptied. Right now, in NFPA 2, the same bulk storage setback distance requirements apply to the storage tank and transfer point. However, if additional data were available on the likelihood of leaks from a stationary tank compared to a transfer point, then the two portions of the system could be treated separately. This could potentially lead to a reduction in setback distances and other requirements for the stationary storage tank itself, and potentially highlight other mitigations or requirements that should be added to the transfer point specifically.

7.3.2. Explicit Consideration of Mitigations and Uncertainty

Directly incorporating the effect of passive and active mitigations would also help improve this analysis for future requirements. Passive mitigations such as insulated portions of the system and fire-barrier walls are currently included in code language to reduce the setback distances, but these reductions were not explicitly included in the analysis described here. While there is no reason to think that previously accepted reductions due to passive mitigations would not be applicable, it could still add important nuance and clarity to the overall analysis to add these effects. There may be some situations in which the mitigations offer more or less protection than in others, and that would be important to consider for future requirements. Additionally, active mitigations such as an automatic shutoff valve were discussed in this work, but not directly included in the numerical results. While it can be difficult to quantify the direct effect of an automatic shutoff valve, including the effect of one in a probabilistic way may still add important insights as to where or how such a device might offer additional protections. By including the effects of passive and active mitigations directly in the basis for, or calculation of, the setback distance values, the effects of these mitigations could be more fully understood and more accurately incorporated into prescriptive requirements.

The leak size basis for this analysis was determined primarily through sensitivity studies on risk assessment results. Many of these risk assessments include some probabilistic effects, but in other cases use deterministic inputs that were varied in a couple dozen sensitivity cases. While this was indeed useful and led to important insights, a better and more complete picture of the uncertainty throughout the risk assessment calculation may improve the validity of the overall justification. This

could include a broader and more formalized way to include various sensitivity cases, or may include propagation of uncertainty in the parameters themselves through the risk estimation. There are many ways in which this could be done, but including more nuance in the uncertainty in the analysis may lead to improved justifications for these types of risk-informed requirements. Additionally, the current analysis relied on a steady-state leak assumption rather than focusing on the storage volume or capacity. While this may be a conservative assumption in some cases, very large-scale capacity storage may lead to cascade failures or more serious consequences that should be considered. Future analyses should explicitly consider how the storage capacity does (or does not) contribute to changes in the risk and how this may affect prescriptive requirements. Very large storage systems are in fact, not explicitly covered by these setback distances, but with expansion of the hydrogen economy may become more common and should therefore have a codified basis for siting.

7.3.3. Application of Methodology to Other Systems

Finally, while there are certainly ways in which this analysis itself could be improved, it is also worth considering how this analysis could be applied to other types of systems and other requirements. The overall structure of this analysis was based on prior work done for bulk gaseous hydrogen storage, but this analysis did make some different assumptions in the analysis and justifications. Applying this same (or very similar) analysis to a bulk gaseous hydrogen storage system could lead to improvements in the setback distance requirements for that type of system. Additionally, NFPA 2 treats refueling dispensers and non-bulk (small capacity) storage differently for both gaseous and liquid hydrogen. While some different considerations and assumptions may need to be made in those cases, applying an overall similar methodology could improve the requirements for those systems and help make the NFPA 2 code overall more consistent. There are many ways in which prescriptive code requirements can be determined and justified, but using a well-documented, retrievable, repeatable, revisable, independently-verified, and experimentally-validated methodology will almost certainly always be useful.

This page left blank

REFERENCES

1. NFPA 2, "Hydrogen Technologies Code," National Fire Protection Association, 2020.
2. J. LaChance, W. Houf, B. Middleton, and L. Fluer, "Analyses to Support Development of Risk-Informed Separation Distances for Hydrogen Codes and Standards," SAND2009-0874, Sandia National Laboratories, March 2009.
3. B.D. Ehrhart, C. Sims, E.S. Hecht, B.B. Schroeder, K.M. Groth, J.T. Reynolds, and G.W. Walkup, "HyRAM+ (Hydrogen Plus Other Alternative Fuels Risk Assessment Models), Version 4.1," software available at: https://hyram.sandia.gov, Sandia National Laboratories, April 29, 2022.
4. E.S. Hecht and B.D. Ehrhart, "Hydrogen Plus Other Alternative Fuels Risk Assessment Models (HyRAM+) Version 4.1: Technical Reference Manual," SAND2022-5649, Sandia National Laboratories, April 2022.
5. CGA P-28, "OSHA process safety management and EPA risk management plan guidance document for bulk liquid hydrogen supply systems," Compressed Gas Association, 2014.
6. D.M. Brooks, B.D. Ehrhart, and C. LaFleur, "Development of liquid hydrogen leak frequencies using a Bayesian update process," in 2021 International Conference on Hydrogen Safety, September 2021.
7. S. Jallais, E. Vyazmina, D. Miller, and J. K. Thomas, "Hydrogen jet vapor cloud explosion: A model for predicting blast size and applilcation to risk assessment," *Process Safety Process,* vol. 37, no. 3, pp. 397-410, 2018.
8. K. Lyons, S. Coldrick, and G. Atkinson, "Summary of experiment series e3.5 (rainout) results," Technical Report available at https://hysafe.info/wp-content/uploads/sites/3/2020/08/PRESLHY_D3.6_Summary_of_Rainout_Experiments_V1.20.pdf, 2020.
9. M. Huescar, A. Halford, and J. Stene, "Liquid Hydrogen Safety Data Report: Outdoor leakage study," DNV-GL. Report # 853182, Rev. 2, 2020.
10. TNO Green Book, "Methods for the Determination of Possible Damage," Netherlands: Director-General of Labor, 1992.
11. P.K. Raj, "A review of the criteria for people exposure to radiant heat flux from fires," *Journal of Hazardous Materials,* vol. 159, pp. 61-71, 2008.
12. J. LaChance, A. Tchouvelev, and A. Engebo, "Development of uniform harm criteria for use in quantitative risk analysis of the hydrogen infrastructure," *International Journal of Hydrogen Energy,* vol. 36, no. 3, pp. 2381-2388, 2011.
13. J. Grune, K. Sempert, M. Kuznetsov, and T. Jordan "Hydrogen Jet Structure in Presence of Forced Co-, Counter- and Cross-Flow Ventilation" Presented at the International Conference on Hydrogen Safety (ICHS) 2021, September 21-24.
14. W. Houf and R. Schefer, "Predicting radiative heat fluxes and flammability envelopes from unintended releases of hydrogen," *International Journal of Hydrogen Energy,* vol. 32, pp. 136-151, 2007.
15. I.W. Ekoto, A.J. Ruggles, L.W. Creitz, and J.X. Li, "Updated jet flame radiation modeling with buoyancy corrections," *International Journal of Hydrogen Energy,* vol. 39, pp. 20570-20577, 2014.
16. B.D. Ehrhart, E.S. Hecht, and J.A. Mohmand, "Validation and Comparison of HyRAM Physics Models," SAND2021-5811, Sandia National Laboratories, May 2021.
17. M. Royle and D. Willoughby, "Releases of unignited liquid hydrogen," Technical Report RR986, Health and Safety Laboratory, 2014.

18. DNV GL Oil and Gas, "Liquid hydrogen safety data report: Outdoor leakage studies," Technical Report 853182, Forsvarets forskningsinstitutt (FFI) Norwegian Defence Research Establishment, available at https://www.vegvesen.no/_attachment/2997130/binary/1373429, 2020.
19. NFPA 59A, "Standard for the Production, Storage, and Handling of Liquified Natural Gas (LNG)," National Fire Protection Association, 2019.
20. M.R. Swain, P.A. Filoso, and M.N. Swain, "An experimental investigation into the ignition of leaking hydrogen," *International Journal of Hydrogen Energy,* vol. 32, no. 2, pp. 287-295, 2007.
21. R.W. Schefer, G.H. Evans, J. Zhang, A.J. Ruggles, and R. Greif, "Ignitability limits for combustion of unintended hydrogen releases: Experimental and theoretical results," *International Journal of Hydrogen Energy,* vol. 36, no. 3, pp. 2426-2435, 2011.
22. A.J. Ruggles and I.W. Ekoto, "Ignitability and mixing of underexpanded hydrogen jets," *International Journal of Hydrogen Energy,* vol. 37, no. 22, pp. 17549-17560, 2012.
23. J. LaChance, A. Tchouvelev, and A. Engebo, "Development of uniform harm criteria for use in quantitative risk analysis of the hydrogen infrastructure," *International Journal of Hydrogen Energy,* vol. 36, no. 3, pp. 2381-2388, 2011.
24. J. Lobato, R. Juan, J. Carlos, L. Javier, N.-M. Antonio, and I. Antonio, "Consequence analysis of an explosion by simple models: Texas refinery gasoling explosion case," *Afinidad,* vol. 66, no. 543, 2009.
25. Quest Consultants Inc., "Preliminary Quantitative Risk Analysis (QRA) of the Texas Clean Energy Project," available at https://netl.doe.gov/sites/default/files/environmental-policy/eis-texas/TCEP-DEIS-Appendix-C---TCEP_Final_Risk_Analysis.pdf, 2010.
26. U.K. Health and Safety Executive, "Methods of approximation and determination of human vulnerability for offshore major accident hazard assessment," available at https://www.hse.gov.uk/foi/internalops/hid_circs/technical_osd/spc_tech_osd_30/spctecosd30.pdf, 2010.
27. Y. Huang and G. Ma, "A grid-based risk screening method for fire and explosion events of hydrogen refueling stations," *International Journal of Hydrogen Energy,* vol. 43, no. 1, pp. 442-454, 2018.
28. T. Argo and E. Sandstrom, "Separation Distances in NFPA Codes and Standards," Techical Report, The Fire Projection Research Foundation, 2014.
29. G. Hankinson and B.J. Lowesmith, "A consideration of methods of determining the radiative characteristics of jet fires," *Combustion and Flame,* vol. 159, no. 3, pp. 1165-1177, 2012.
30. W.G. Houf, G.H. Evans, R.W. Schefer, E. Merilo, and M. Groethe, "A study of barrier walls for mitigation of unintended releases of hydrogen," *International Journal of Hydrogen Energy,* vol. 36, pp. 250-259, 2011.
31. J. LaChance, J. Philips, and W. Houf, "Risk associated with the use of barriers in hydrogen refueling stations," in *Annual Hydrogen Conference and Hydrogen Expo USA*, 2010.
32. K. Groth, C. San Marchi, W. James, and K. Kiuru, "Separation distance reduction based on risk-informed analysis," DOE Hydrogen and Fuel Cells Program Record, May 12 2015.
33. R.W. Schefer, M. Groethe, W.G. Houf, and G. Evans, "Experimental evaluation of barrier walls for risk reduction of unintended hydrogen releases," *International Journal of Hydrogen Energy,* vol. 34, pp. 1590-1606, 2009.
34. M.J. Hurley, Ed., "SFPE Handbook of Fire Protection Engineering," vol. 5 ed., Springer, 2016.

35. J. Daycock and P. Rew, "Development of a method for the determination of on-site ignition probabilities," Research Report 226, U.K. Health and Safety Executive (HSE), 2004.
36. A.V. Tchouvelev, "Knowledge gaps in hydrogen safety: A white paper," International Energy Agency Implementating Agreement Task 19, January 2008.
37. P. Virtanen, R. Gommers, T.E. Oliphant, M. Haberland, T. Reddy, D. Cournapeau, E. Burovski, P. Peterson, W. Weckesser, J. Bright, S.J. van der Walt, M. Brett, J. Wilson, K.J. Millman, N. Mayorov, A.R.J. Nelson, E. Jones, R. Kern, E. Larson, C.J. Carey, I. Polat, Y. Feng, E.W. Moore, J. VanderPlas, D. Laxalde, J. Perktold, R. Cimrman, I. Henriksen, E.A. Quintero, C.R. Harris, A.A. Archibald, A.H. Ribeiro, F. Pedregosa, P. van Mulbregt, and Scipy 1.0 Contributors, "SciPy 1.0: Fundamental Algorithms for Scientific Computing in Python," *Nature Methods,* vol. 17, pp. 261-272, 2020.
38. Bluebeam Revu Software, available at: https://www.bluebeam.com/solutions/revu.
39. Acme Cryogenics, "QCI Style Bayonets," available at: https://www.acmecryo.com/wp-content/uploads/2021/04/CLOSE-TOLERANCE-BAYONETS_SELL_SHEET-1.pdf.
40. Cryocomp, "B3000 Series: Cryogenic Bayonet for Vacuum Insulated Piping Systems," available at: https://www.cryocomp.com/products/cryogenic-bayonet-b3000-series/.
41. CPC-Cryolab, "Bayonet Connections: Vacuum Insulated Cryogenic Connections," available at: https://cpc-cryolab.com/wp-content/uploads/Bayonet.pdf.

This page left blank

APPENDIX A. DETAILS OF RISK-INFORMED EQUIVALENT HOLE SIZE CALCULATIONS

Additional supporting information for Section 2.1 is provided within this appendix.

A.1. Constant Parameter Values used in QRA

Many parameters input into the QRA calculations in the HyRAM+ toolkit were varied from their nominal values during the sensitivity study, while other parameters were kept the same values throughout the analysis. Table 8 shows the parameter values that remained fixed throughout the analyses.

Table 8: Constant parameters in QRA analysis

Parameter	Value
Ambient temperature	20.0°C
Ambient pressure	14.7 psia
Nozzle model	Yuce
Exclusion radius	0.01 m
Leak frequency distributions	From [4]*
Dispenser failure	False

** GH2 defaults used for compressor, instrument, filter*

It should be noted that wind speed was only used for the equivalent hole size calculations for the jet flame, in which a constant 5 m/s wind speed was used. The wind speed does not affect the risk calculations, nor does it affect any other calculation aside from the momentum of the jet flame. This is only available in the back-end Python-only version of HyRAM+ 4.1, not through the front-end graphical user interface.

A.2. Representative LH2 System

To determine appropriate part counts for the representative LH2 system, the CGA P-28 2014 typical LH2 system was analyzed [5]. Each component was determined to either interact with LH2, interact with GH2, or be under vacuum, as shown in Figure 20. Only components that interact with LH2 were included in the analysis parts count, as shown in Table 9.

Table 9: Parts counts of representative LH2 system

Component	Count
Compressors	1
Pipes	10

Component	Count
Vessels	1
Filters	2
Valves	44
Flanges	8
Instruments	3

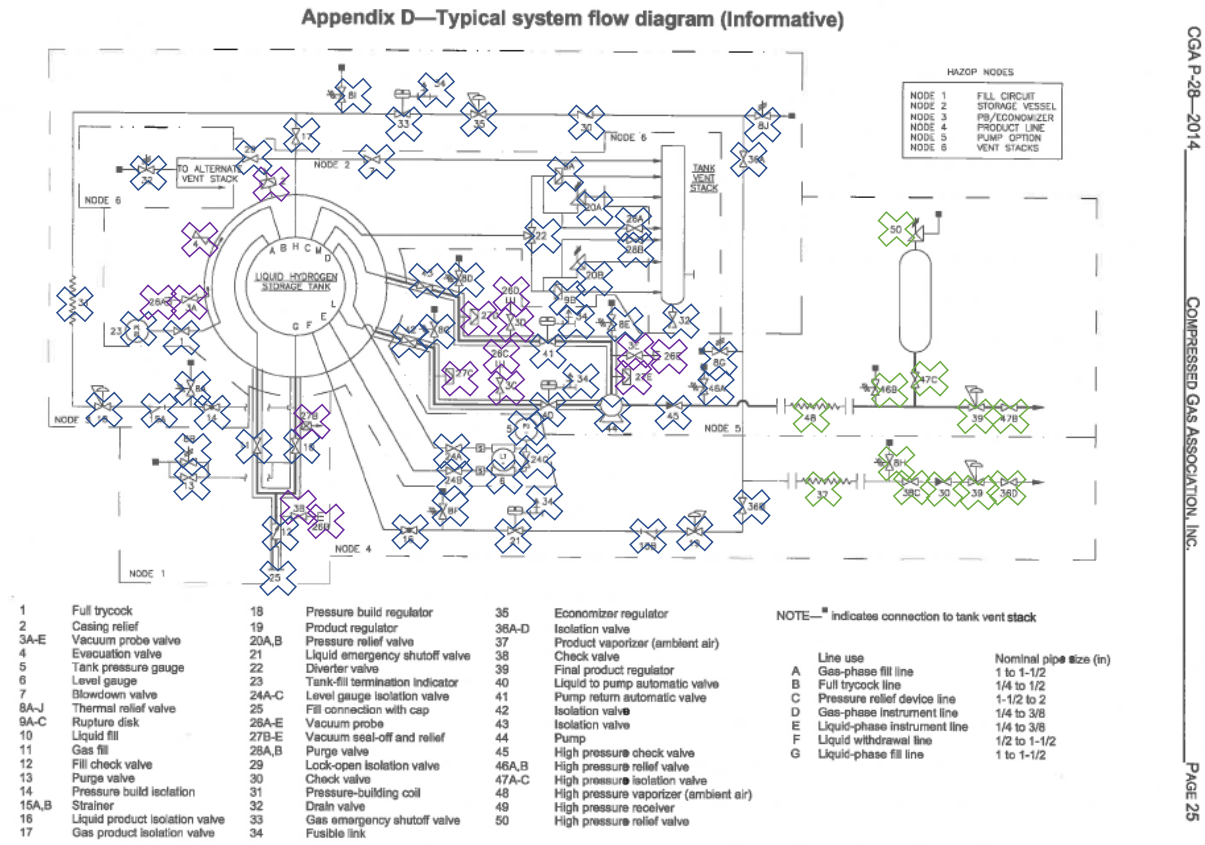


Figure 20: CGA P-28 2014 typical system flow diagram [5] adopted as representative LH2 system for QRA calculations. Blue symbols indicate LH2 components, green symbols indicated GH2 components, and purple symbols indicated components under vacuum.

A.3. Discontinuities in Equivalent Fractional Hole Size Responses

Within the equivalent fractional hole size (EFHS) curves, such as in Figure 6, discontinuities are present. These discontinuities were due to the ignition probabilities, which are shown in Table 10. Ignition probabilities are specified based on mass flow rate and are step functions at the specified mass flow rate thresholds. Figure 21 demonstrates how the mass flow rate for each leak size is a

smooth function of pipe inner diameter, but when the flow rate from one of the leak sizes increases beyond one of the ignition probability mass flow rate thresholds, a jump occurs in the respective ignition probabilities. The discontinuities in ignition probabilities are propagated through the risk assessment, resulting in discontinuities in the calculated risk metrics, the risk-based distances, and ultimately the EFHS function curves.

Table 10: Ignition Probabilities [36]

Mass flow rate (kg/s)	Immediate Ign. Prob.	Delayed Ign. Prob.
≤ 0.125	0.008	0.004
0.125 > x ≤ 6.2	0.053	0.027
> 6.25	0.23	0.12

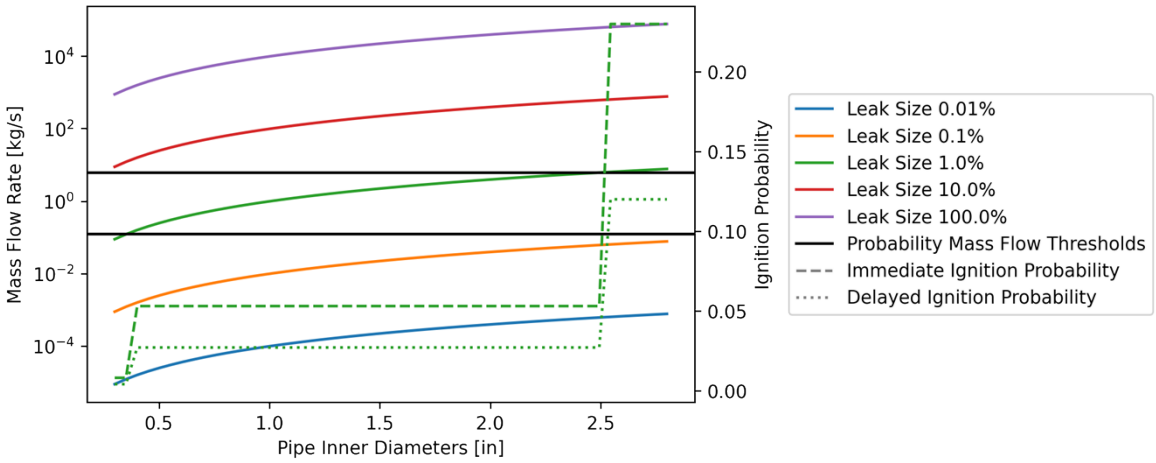


Figure 21: Demonstration of how discontinuities in mass flow rate based ignition probabilities cause jumps in ignition probability over pipe diameter range considered for the QRA analysis. Ignition probabilities only shown for 10.0% leak size.

A.4. Consequence-Based Equivalent Hole Size Calculation

To solve for consequence-based equivalent hole sizes, the root finding algorithm for scalar functions was utilized from the Python package SciPy [37]. The root finding algorithm required three inputs: a function to evaluate, bounds for the scalar parameter within which the root should be located, and the respective consequence metric value. The function was specified as a consequence model that evaluated the consequence for a specific distance and hole size. The consequence result returned by the consequence model had the consequence metric subtracted off, that difference was normalized by the consequence metric, and the resulting value was returned to the root finding algorithm. Bounds for the hole size were specified as around 3E-6 and 1.5 m and the respective consequence metric, as shown in Table 2, was used. Due to bounds being specified, SciPy utilizes the brentq

method to solve for the root. Ultimately, the root finding algorithm returned the hole size for which the consequence model's prediction matched the consequence metric, at a specified distance.

A.5. Consequence Model Sensitivity

Although the sensitivity study that informed the selection of an EFHS explored uncertainty in the QRA calculation, uncertainty can also be explored in the consequence calculations themselves. Figure 22, Figure 23, and Figure 24 demonstrate the sensitivity of consequence based equivalent hole sizes for a range of distances.

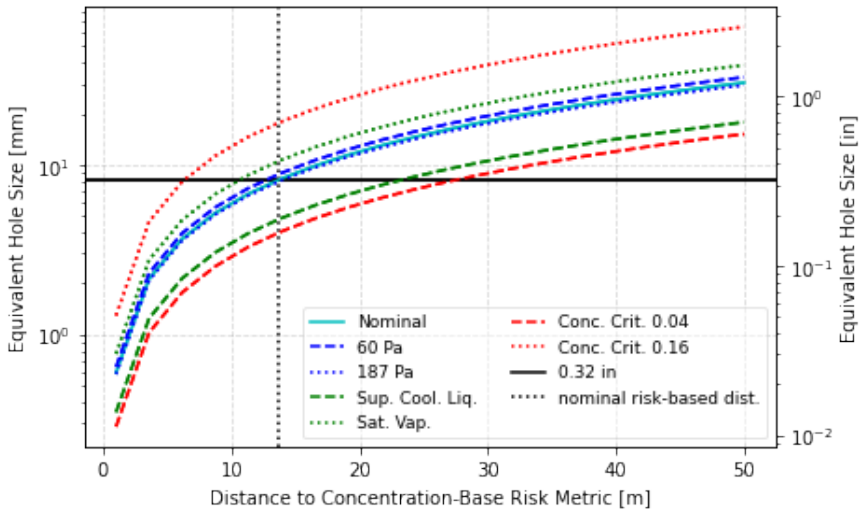


Figure 22: Equivalent hole size as a function of setback distances while varying a range of parametesr impacting concentration metric based risk calculations.

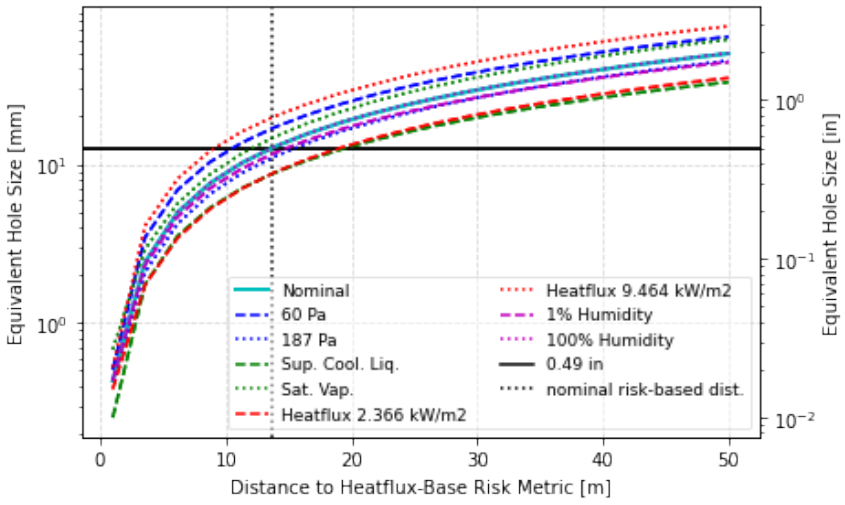


Figure 23: Equivalent hole sizes as a function of setback distances while varying a range of parameters impacting heat flux metric based risk calculations

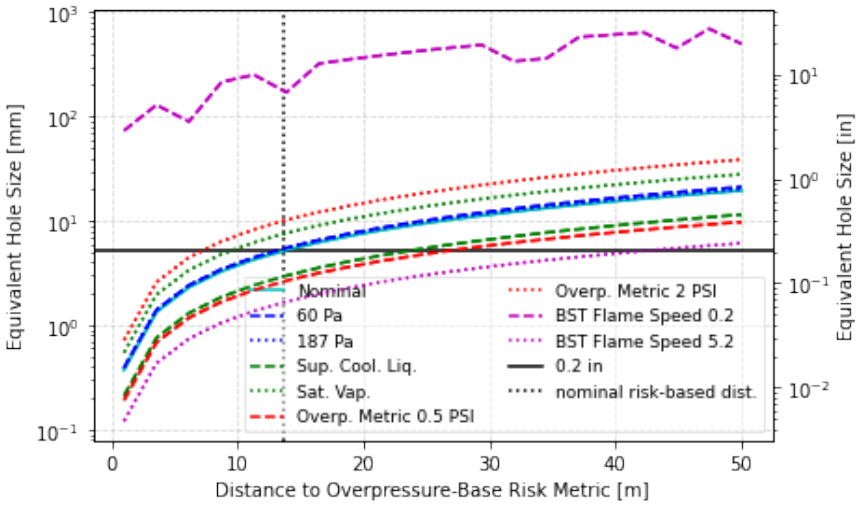


Figure 24: Equivalent hole sizes as a function of setack distances while varying a range of parameters impacting heat flux metric based risk calculations

A.6. Tabulated Equivalent Fractional Hole Size Results

Equivalent Fractional Hole Size (Area-Based) [%]

Pipe Inner Diameter [in]	Nominal	60 psi	187 psi	Sat. Vap.	Sup. Cool Liq.	Humidity 1pct	Humidity 100pct	Risk Metric Half	Risk Metric Double	Detection Credit 0pct	Detection Credit 95pct	BST Mach Flame Speed 0p2	BST Mach Flame Speed 5p2	Exposure Time Half	Exposure Time Double	Component Count Half	Component Count Double	Ignition Probabilities Half	Ignition Probabilities Double	Overpressure Method TNT	Overpressure Method Bauwens	Discharge Coefficient Half	Thermal Probit Tsao and Perry	Thermal Probit TNO	Overpressure Probit Eisenberg	Overpressure Probit HSE
0.3	0.517	0.116	0.970	0.488	0.773	0.578	0.514	0.517	0.517	0.595	0.222	0.517	2.044	0.266	1.091	0.438	0.595	0.438	0.595	0.517	1.543	0.211	1.255	0.871	0.517	0.538
0.404	0.648	0.269	1.180	0.907	1.041	0.748	0.643	0.648	0.648	0.752	0.264	0.648	2.781	0.321	1.404	0.545	0.752	0.544	0.752	0.648	2.102	0.430	1.619	1.115	0.648	0.675
0.508	0.762	0.324	1.347	1.006	1.279	0.902	0.756	0.762	0.762	0.888	0.298	0.762	3.511	0.366	1.677	0.637	0.888	0.636	0.888	0.762	2.548	0.489	1.934	1.328	0.762	0.795
0.613	0.864	0.373	1.486	1.083	1.494	1.044	0.856	0.864	0.864	1.010	0.328	0.864	4.059	0.406	1.917	0.719	1.010	0.718	1.010	0.864	2.865	0.538	2.212	1.518	0.864	0.902
0.717	0.955	0.416	1.606	1.145	1.693	1.175	0.946	0.955	0.955	1.119	0.353	0.955	4.542	0.440	2.131	0.792	1.119	0.792	1.119	0.955	3.276	0.580	2.457	1.687	0.955	0.998
0.821	1.037	0.454	1.714	1.196	1.883	1.296	1.027	1.037	1.037	1.217	0.374	1.037	4.995	0.470	2.321	0.858	1.217	0.857	1.217	1.037	3.469	0.616	2.674	1.838	1.037	1.084
0.925	1.110	0.489	1.811	1.239	2.064	1.407	1.100	1.110	1.110	1.305	0.393	1.110	5.372	0.496	2.490	0.917	1.305	0.916	1.305	1.110	3.542	0.648	2.867	1.973	1.110	1.188
1.029	1.177	0.520	1.900	1.277	2.237	1.509	1.165	1.177	1.177	1.384	0.409	1.177	5.712	0.520	2.641	0.970	1.384	0.969	1.384	1.177	3.652	0.678	3.039	2.094	1.177	1.259
1.133	1.237	0.550	1.981	1.311	3.487	1.604	1.224	1.237	1.237	1.456	0.424	1.237	6.056	0.541	2.777	1.018	1.456	1.017	1.456	1.237	4.123	0.705	3.194	2.203	1.237	1.324
1.238	1.292	0.579	2.055	1.342	3.709	1.691	1.278	1.292	1.292	1.522	0.437	1.292	6.392	0.560	2.901	1.062	1.522	1.061	1.522	1.292	4.388	0.730	3.333	2.303	1.292	1.382
1.342	1.343	0.606	2.123	1.370	3.922	1.774	1.328	1.343	1.343	1.583	0.449	1.343	6.822	0.578	3.013	1.103	1.583	1.102	1.583	1.343	4.593	0.754	3.461	2.394	1.343	1.436
1.446	1.391	0.633	2.185	1.397	4.125	1.852	1.375	1.391	1.391	1.640	0.460	1.391	7.357	0.595	3.118	1.141	1.640	1.141	1.640	1.391	4.709	0.777	3.579	2.479	1.391	1.486
1.55	1.436	0.659	2.243	1.422	4.319	1.926	1.419	1.436	1.436	1.693	0.471	1.436	7.917	0.611	3.215	1.178	1.693	1.177	1.693	1.436	4.885	0.799	3.689	2.558	1.436	1.534
1.654	1.479	0.684	2.297	1.446	4.504	1.997	1.461	1.479	1.479	1.744	0.482	1.479	8.232	0.626	3.307	1.213	1.744	1.212	1.744	1.479	4.901	0.819	3.792	2.632	1.479	1.578
1.758	1.519	0.708	2.347	1.469	4.682	2.065	1.501	1.519	1.519	1.791	0.492	1.519	8.424	0.641	3.393	1.246	1.791	1.245	1.791	1.519	4.964	0.839	3.889	2.703	1.519	1.620
1.863	2.149	0.732	3.175	1.490	4.852	2.932	2.123	2.149	2.149	2.431	1.218	2.149	8.888	0.918	4.611	1.871	2.431	1.870	2.431	2.149	8.876	0.858	5.246	3.719	2.149	2.649
1.967	2.200	0.756	3.233	1.510	5.016	3.015	2.173	2.200	2.200	2.487	1.247	2.200	9.138	0.939	4.710	1.915	2.487	1.914	2.487	2.200	9.234	0.876	5.357	3.802	2.200	2.711
2.071	2.249	0.778	3.287	1.529	5.173	3.096	2.220	2.249	2.249	2.542	1.275	2.249	9.440	0.960	4.804	1.958	2.542	1.957	2.542	2.249	9.499	0.893	5.462	3.880	2.249	2.848
2.175	2.296	0.801	3.338	1.547	5.325	3.174	2.267	2.296	2.296	2.594	1.302	2.296	9.727	0.980	4.895	2.000	2.594	1.999	2.594	2.296	9.601	0.910	5.563	3.956	2.296	2.907
2.278	2.342	1.177	3.387	1.565	5.471	3.251	2.312	2.342	2.342	2.646	1.330	2.342	10.003	1.000	4.983	2.041	2.646	2.040	2.646	2.342	9.735	0.926	5.661	4.029	2.342	2.962
2.383	2.387	1.206	3.434	1.581	5.612	3.325	2.356	2.387	2.387	2.696	1.356	2.387	10.276	1.020	5.068	2.080	2.696	2.079	2.696	2.387	9.907	0.941	5.756	4.101	2.387	3.016
2.488	2.431	1.235	3.479	1.597	5.749	3.398	2.399	2.431	2.431	2.744	1.382	2.431	10.533	1.040	5.150	2.119	2.744	2.118	2.744	2.431	9.856	0.955	5.847	4.170	2.431	3.069
2.592	2.473	1.263	3.522	2.080	5.882	3.469	2.440	2.473	2.473	2.791	1.408	2.473	10.787	1.059	5.230	2.157	2.791	2.156	2.791	2.473	9.899	0.969	5.936	4.236	2.473	3.119
2.692	2.514	1.290	3.565	2.099	6.010	3.539	2.481	2.514	2.514	2.837	1.433	2.514	11.032	1.078	5.307	2.194	2.837	2.193	2.837	2.514	9.945	1.330	6.022	4.301	2.514	3.169
2.8	2.555	1.316	3.605	2.116	6.135	3.607	2.521	2.555	2.555	2.882	1.457	2.555	11.264	1.096	5.383	2.230	2.882	2.229	2.882	2.555	9.984	1.348	6.106	4.365	2.555	3.217

Figure 25: Tabulated equivalent fractional hole sizes over a range of inner pipe diameter results. Results correspond to lines shown in Figure 6. Colors are a visual guide to higher (blue) and lower (red) values.

This page left blank

APPENDIX B. DETAILS OF BAYONET CONNECTOR LEAK GEOMETRY

Additional details for Section 2.2 are provided here.

B.1. Methodology

There are many different potential failure modes and mechanisms for the connection of a liquid hydrogen transfer point. Typically, these types of connections are made using a bayonet-style connector; an example schematic of a bayonet style connector is shown in Figure 26. Within this type of connector, the cold-seal could fail, leading to a leak of liquid hydrogen. This could be due to misalignment, failure of the seal material, and many other factors. In any case, the liquid hydrogen would then travel along the annulus of the bayonet connector and encounter the O-ring on the sealing flange. The cryogenic temperatures of the hydrogen would likely cause this O-ring to fail and leak the hydrogen. Therefore, the release of hydrogen through the O-ring area is the scenario being considered here. There are many mechanisms that could cause hydrogen to leak out of the O-ring, but that is the final point at which the hydrogen would be released into the surrounding air.

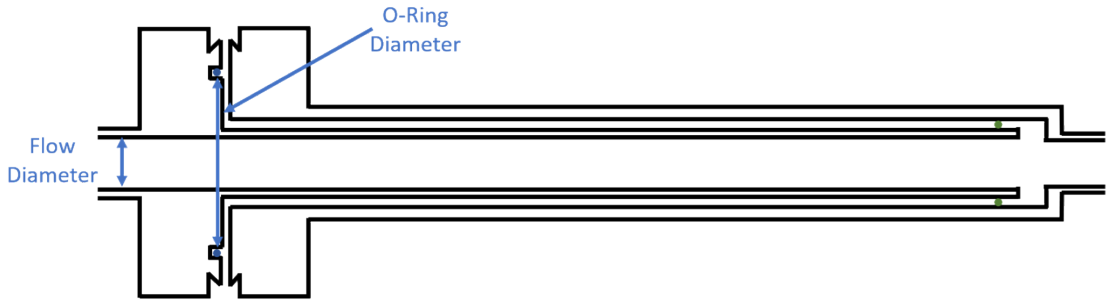


Figure 26: Example schematic of a bayonet-style connector used in the transfer of liquid hydrogen

Different manufacturers have different styles of bayonet connectors, as well as different sizes (diameters) of connectors. A number of commercially-available connectors were identified that listed some of the relevant dimensions of their connectors in the associated sales literature. The exact dimensions of interest were not always given in the published materials; therefore, estimates of the dimensions of interest were made by comparing the measurements of the published schematics with dimensions that were published in the sales literature. The measurements were done using the Bluebeam Revu software [38]. It should be noted that these measurements are not exact, as they are rough estimates based on sales literature, not engineering drawings. However, the obtained leak sizes can still be of use, especially in the determination of trends.

The O-ring diameter obtained from the literature (d_{o-ring}) is then used to calculate the flow area (A_{o-ring}) as shown in Equation 2. The O-ring gap height (δ_{o-ring}) is assumed to be 0.1 mm (0.004 in) based on discussions with liquid hydrogen industry experts. This gap height is not the height or diameter of the O-ring itself, but rather the gap between the flanges of the seal; in a properly installed system, this height should be very close to zero. It should also be noted that this area calculation assumes that the O-ring fails completely, meaning that the entire flow area around the circumference of the O-ring allows for flow. In reality, it is likely that a leak would flow from a rupture on part of the O-ring, meaning that flow is blocked for part of the circumference.

$$A_{o-ring} = \pi d_{o-ring} \delta_{o-ring} \quad \text{Equation 2}$$

The flow area for the bayonet connector (A_{flow}) is the inner cross-sectional area through which liquid hydrogen is intended to flow. It is calculated as the area of a circle based on the flow area diameter obtained from the literature (d_{flow}) as shown in Equation 3.

$$A_{flow} = \frac{\pi}{4} d_{flow}^2 \quad \text{Equation 3}$$

Finally, the leak area (A_{o-ring}) is compared to the flow area (A_{flow}) to get the fractional leak size (f_{leak}) as calculated in Equation 4.

$$f_{leak} = \frac{A_{o-ring}}{A_{flow}} \quad \text{Equation 4}$$

B.2. Results and Discussion

The various bayonet connectors, obtained diameters, and calculated leak area fractions (using Equation 2 through Equation 4) are shown in Table 11.

Table 11: Bayonet connector diameters and leak area fractions for O-ring failure

Manufacturer	Part Number	Ref.	Type	O-Ring Diameter (d_{o-ring})		Flow Diameter (d_{flow})		O-Ring Gap Area Fraction of Flow Area (%) (f_{leak})
				mm	in	mm	in	
ACME	0.5 IPS sch 5	[39]	Male	33.0	1.3	12.7	0.5	8.2
ACME	1 IPS sch 5	[39]	Male	50.8	2.0	25.4	1.0	3.1
ACME	1.5 IPS sch 10	[39]	Male	57.2	2.2	38.1	1.5	1.6
ACME	2 IPS sch 10	[39]	Male	64.0	2.5	50.8	2.0	1.0
Cryocomp	B3049-MB	[40]	Male	53.3	2.1	21.6	0.8	4.6
Cryocomp	B30412-MB	[40]	Male	53.3	2.1	21.6	0.8	4.6
Cryocomp	B3069-MB	[40]	Male	53.3	2.1	27.2	1.1	2.9
Cryocomp	B30612-MB	[40]	Male	53.3	2.1	27.2	1.1	2.9
Cryocomp	B30812-MB	[40]	Male	58.4	2.3	33.5	1.3	2.1
Cryolab-AF	F-BMAFPS12X	[41]	Male	101.6	4.0	48.3	1.9	1.7
Cryolab-AF	F-BMAFTS12X	[41]	Male	101.6	4.0	38.1	1.5	2.8
Cyrolab-Lin	F-BFLTPS16X	[41]	Female	78.7	3.1	60.5	2.4	0.9
Cyrolab-Lin	F-BFLTTS16X	[41]	Female	78.7	3.1	50.8	2.0	1.2
Cyrolab-Lin	F-BFLTPS12X	[41]	Female	78.7	3.1	33.0	1.3	2.9
Cyrolab-Lin	F-BFLTTS12X	[41]	Female	78.7	3.1	25.4	1.0	4.9

Manufacturer	Part Number	Ref.	Type	O-Ring Diameter (d_{o-ring})		Flow Diameter (d_{flow})		O-Ring Gap Area Fraction of Flow Area (%) (f_{leak})
				mm	in	mm	in	
Cyrolab	F-BMCTPS04X	[41]	Male	54.6	2.2	21.3	0.8	4.8
Cyrolab	F-BMCTPS08X	[41]	Male	66.0	2.6	33.3	1.3	2.4
Cyrolab	F-BMCTPS12X	[41]	Male	81.3	3.2	48.3	1.9	1.4
Cyrolab	F-BMCTPS16X	[41]	Male	104.1	4.1	60.2	2.4	1.1
Cyrolab	F-BMCTPS24X	[41]	Male	129.5	5.1	88.9	3.5	0.7
Cyrolab	F-BMCTPS32X	[41]	Male	152.4	6.0	114.3	4.5	0.5
Cyrolab	F-BMCTPS48X	[41]	Male	248.9	9.8	168.1	6.6	0.4

The fractional leak areas are compared to the inner flow diameters in Figure 27. This indicates that the fractional leak area tends to decrease with increasing flow diameters. Mathematically, this makes sense, as the calculations above were based on the assumption of a constant O-ring gap height. However, there is no reason to believe that larger diameter connectors would have a different flange gap separation, so this assumption seems reasonable.

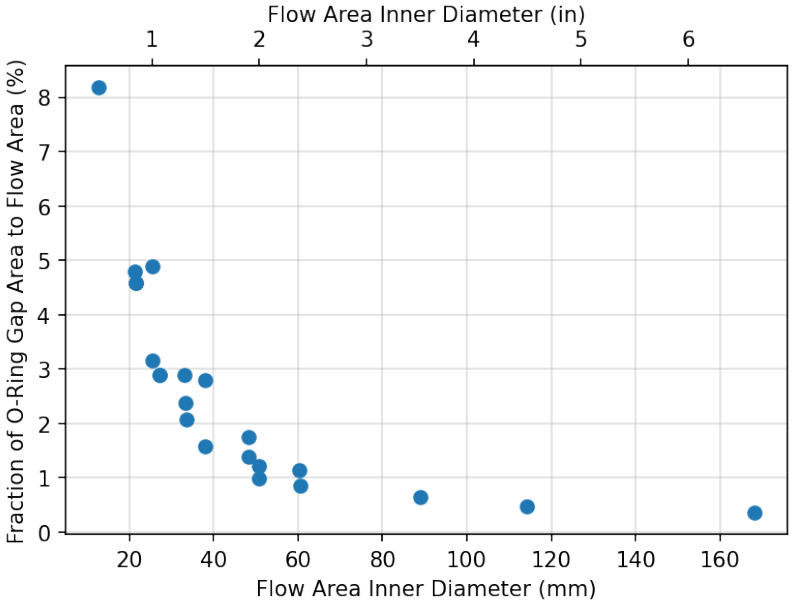


Figure 27: Fractional leak area based on O-ring failure of bayonet connector compared to corresponding inner flow diameter

This page left blank

DISTRIBUTION

Email—Internal

Name	Org.	Sandia Email Address
Ethan Hecht	8367	ehecht@sandia.gov
Kristin Hertz	8367	klhertz@sandia.gov
Dusty Brooks	8854	dbrooks@sandia.gov
Brian Ehrhart	8854	bdehrha@sandia.gov
Chris LaFleur	8854	aclafle@sandia.gov
Benjamin Schroeder	8854	bbschro@sandia.gov
Technical Library	1911	sanddocs@sandia.gov

Email—External

Name	Company Email Address	Company Name
John Anicello	john.anicello@chartindustries.com	Chart Industries
Thomas Drube	tom.drube@chartindustries.com	Chart Industries
David Farese	faresedj@airproducts.com	Air Products
Laura Hill	laura.hill@ee.doe.gov	DOE HFTO
Derek Miller	millerd3@airproducts.com	Air Products
Jamal Mohmand	jamal.a.mohmand@lmco.com	Lockheed Martin (formerly Sandia National Labs)
Mukesh Trivedi	mukesh.trivedi@chartindustries.com	Chart Industries

This page left blank

This page left blank



Sandia National Laboratories

Sandia National Laboratories is a multimission laboratory managed and operated by National Technology & Engineering Solutions of Sandia LLC, a wholly owned subsidiary of Honeywell International Inc. for the U.S. Department of Energy's National Nuclear Security Administration under contract DE-NA0003525.